

Phase boundaries of power-law Anderson and Kondo models: A poor man's scaling study

Mengxing Cheng,^{1,2} Tathagata Chowdhury,^{1,3,*} Aaron Mohammed,^{1,4} and Kevin Ingersent¹

¹*Department of Physics, University of Florida, P.O. Box 118440, Gainesville, Florida 32611-8440, USA*

²*Research Computing Center, University of Chicago,
5607 South Drexel Avenue, Chicago, Illinois 60637, USA*

³*Institut für Theoretische Physik, Universität zu Köln, Zùlpicher Stasse 77a, 507937 Köln, Germany*

⁴*Department of Physics, University of South Florida,
4202 East Fowler Avenue, Tampa, Florida 33620, USA*

(Dated: November 10, 2021)

We use the poor man's scaling approach to study the phase boundaries of a pair of quantum impurity models featuring a power-law density of states $\rho(\varepsilon) \propto |\varepsilon|^r$, either vanishing (for $r > 0$) or diverging (for $r < 0$) at the Fermi energy $\varepsilon = 0$, that gives rise to quantum phase transitions between local-moment and Kondo-screened phases. For the Anderson model with a pseudogap (i.e., $r > 0$), we find the phase boundary for (a) $0 < r < 1/2$, a range over which the model exhibits interacting quantum critical points both at and away from particle-hole (p - h) symmetry, and (b) $r > 1$, where the phases are separated by first-order quantum phase transitions that are accessible only for broken p - h symmetry. For the p - h -symmetric Kondo model with easy-axis or easy-plane anisotropy of the impurity-band spin exchange, the phase boundary and scaling trajectories are obtained for both $r > 0$ and $r < 0$. Throughout the regime of weak-to-moderate impurity-band coupling in which poor man's scaling is expected to be valid, the approach predicts phase boundaries in excellent qualitative and good quantitative agreement with the nonperturbative numerical renormalization group, while also establishing the functional relations between model parameters along these boundaries.

PACS numbers: 71.10.Hf, 72.15.Qm, 73.23.-b, 05.10.Cc

I. INTRODUCTION

The Kondo problem—the question of how an impurity local moment becomes screened at low temperatures by the conduction electrons of a host metal—has been highly influential in stimulating the development of theoretical and numerical methods for treating strongly correlated condensed matter [1]. Perturbative treatments of the spin-flip scattering between local and delocalized spins necessarily break down below a characteristic Kondo temperature scale, giving rise to a complex many-body problem. Nonetheless, much valuable understanding of the Kondo problem has come from perturbative renormalization-group (RG) [2, 3] and perturbative scaling [4, 5] approaches. These were distilled into their simplest form in the poor man's scaling of Anderson [5].

In poor man's scaling, electron states far from the Fermi energy are progressively eliminated as the effective bandwidth is reduced with a compensating adjustment of a dimensionless measure of the effective impurity-band exchange coupling. The evolution of this coupling to ever larger values with decreasing bandwidth is suggestive of approach to a fully screened strong-coupling fixed point, although the scaling approach breaks down once the effective bandwidth drops below the order of the Kondo temperature. More sophisticated but generally less intuitive methods (the first historically being the numerical renormalization group or NRG [6]) were

devised to confirm that the infrared fixed point indeed corresponds to infinite exchange [1]. Poor man's scaling was subsequently extended to the Anderson model with impurity Coulomb interaction $U = \infty$ [7, 8] and the n -channel Kondo model [9], where it correctly predicts the existence of a stable RG fixed point at an intermediate value of the exchange coupling that lies within the perturbative domain for $n \gg 2$.

More recently, there has been much interest in Kondo physics in settings where the band density of states has a power-law variation $\rho(\varepsilon) \propto |\varepsilon|^r$ in the vicinity of the Fermi energy $\varepsilon = 0$. Pseudogaps described by exponents $r > 0$ can be found in a variety of materials including heavy-fermion and cuprate unconventional superconductors [10, 11], zero-gap bulk [12] and engineered [13] semiconductors, and various (quasi-)two-dimensional systems such as graphite [14, 15] and graphene [16]. An exponent $r = -\frac{1}{2}$ arises near a band edge in one-dimensional leads, while values $-1 < r < 0$ can describe disordered Dirac fermions in two dimensions [17, 18]. Several theoretical techniques that have proved powerful for describing quantum impurities in metallic hosts, including the Bethe ansatz, bosonization, and conformal field theory, cannot be applied for a power-law density of states. However, power-law variants of the Kondo impurity model and the corresponding Anderson model have been extensively studied using other techniques such as perturbative scaling [19–23], large- N approaches [19, 24–27], the NRG [22, 28–35], the perturbative RG [36–38], and the local-moment approach [39–41]. Due to the depletion of the conduction-band density of states near

* tatha@thp.uni-koeln.de

the Fermi energy, these pseudogap models feature quantum phase transitions [19] between a local-moment phase for weak impurity-band couplings, in which the impurity spin survives unscreened down to zero temperature, and one or more strong-coupling Kondo phases in which the impurity spin undergoes complete or partial many-body screening (depending on the presence or absence of particle-hole symmetry) [31].

Of all the techniques so far applied to the pseudogap Anderson and Kondo models, only the NRG has proved capable of capturing all the key features of the phase diagram, including the existence of four qualitatively different ranges of the band exponent r [31]. However, as is true for many computational methods, the NRG's reliability comes at the price of laborious implementation and a loss of physical transparency. Together, these make it difficult to obtain simple intuition about how two fundamentally opposing tendencies—growth of host correlations engendered by a local dynamical degree of freedom, and the weakening of host-impurity interaction due to depression of the low-energy density of states—compete to create nontrivial temperature dependencies of physical properties and to shape phase boundaries. The local-moment approach [42] reproduces rather well the phase boundaries of the pseudogap Anderson model with band exponents $0 < r < 1$, but its analytical insights are confined to situations of strict particle-hole symmetry [39, 40] or the limit $r \rightarrow 0^+$ [41].

It is highly desirable to identify another primarily analytical approach that can shed light more widely on the functional relations describing the phase boundaries in challenging quantum impurity problems that feature both (i) more than one independent coupling that flows under the reduction of the effective bandwidth, and (ii) unstable quantum critical points arising from competing flows in the multidimensional parameter space of effective couplings. A promising candidate is poor man's scaling [5], which has previously been established to account well for the possible ground states of many quantum impurity problems and to provide an approximate description of the physics on different energy/temperature scales in terms of a flow through a space of renormalized Hamiltonian couplings. The method yields a set of ordinary differential equations describing the renormalization of Hamiltonian couplings. These differential equations can in some cases be integrated in closed form; failing that, their solutions can be explored numerically via numerical iteration from different choices of bare couplings.

In this paper, we critically evaluate the adequacy of poor man's scaling for describing phase boundaries in the Anderson model (with an arbitrary on-site repulsion U) and in the particle-hole-symmetric Kondo model with easy-axis or easy-plane anisotropy of the impurity-band exchange coupling. For each model, we generalize previous treatments to obtain coupled differential equations for the evolution of effective couplings under progressive reduction of the conduction bandwidth. These equations are valid for any density of states of the form

$\rho(\omega) \propto |\omega|^r$, whether r is positive, negative, or zero. (The case $r = 0$ describes conventional metallic hosts.) We obtain analytical expressions for the locations of phase boundaries for different parameter ranges of the pseudogap ($r > 0$) Anderson and power-law ($r \neq 0$) anisotropic Kondo models. Comparison with nonperturbative NRG results shows that throughout the perturbative regime where the method is well-founded, poor man's scaling correctly captures the functional relations between model parameters along various parts of the phase boundaries, and also reproduces the absolute location of the boundaries with good quantitative accuracy. The availability of proven analytical expressions obviates the need for further NRG calculations to understand and make predictions about possible realizations of these models.

The rest of the paper is organized as follows. Section II treats the Anderson model with a power-law density of states. Section II A defines the model and summarizes the phase diagram that has been established through previous work. The poor man's scaling equations are derived in Sec. II B. Section II C compares analytic approximations for the phase boundary with NRG results for super-linear ($r > 1$) densities of states and various ranges of the other model parameters, while Sec. II D does the same for $0 < r < 1$. The anisotropic Kondo model is the subject of Sec. III. Section III A presents the poor man's scaling equations along with a preliminary analysis. Phase boundaries are analyzed for $0 < r < \frac{1}{2}$ and $-1 < r < 0$ in Secs. III B and III C, respectively. Section IV contains a brief discussion of strengths and weaknesses shown by the poor man's scaling approach.

II. POWER-LAW ANDERSON MODEL

A. Model Hamiltonian

The Anderson impurity model is described by the Hamiltonian [43]

$$\hat{H}_A = \hat{H}_{\text{band}} + \hat{H}_{\text{imp}} + \hat{H}_{\text{hyb}}, \quad (1)$$

where

$$\hat{H}_{\text{band}} = \sum_{\mathbf{k}, \sigma} \varepsilon_{\mathbf{k}} c_{\mathbf{k}\sigma}^\dagger c_{\mathbf{k}\sigma} \quad (2)$$

with $\sigma = \pm 1$ (or $\sigma = \uparrow, \downarrow$) describes a noninteracting conduction band having dispersion $\varepsilon_{\mathbf{k}}$;

$$\hat{H}_{\text{imp}} = \varepsilon_d \hat{n}_d + U \hat{n}_{d\uparrow} \hat{n}_{d\downarrow} \quad (3)$$

with $\hat{n}_d = \hat{n}_{d\uparrow} + \hat{n}_{d\downarrow}$ and $\hat{n}_{d\sigma} = d_\sigma^\dagger d_\sigma$ describes an impurity having level energy ε_d and on-site Coulomb interaction U ; and the hybridization term

$$\hat{H}_{\text{hyb}} = \frac{1}{\sqrt{N_k}} \sum_{\mathbf{k}, \sigma} (V_{\mathbf{k}} d_\sigma^\dagger c_{\mathbf{k}\sigma} + \text{H.c.}) \quad (4)$$

accounts for impurity-band tunneling. N_k is the number of unit cells in the host metal, N_k is the number of inequivalent \mathbf{k} values. Without loss of generality, we take the hybridization matrix element $V_{\mathbf{k}}$ to be real and non-negative. For compactness of notation, we drop all factors of the reduced Planck constant \hbar , Boltzmann's constant k_B , and the impurity magnetic moment $g\mu_B$.

A mapping to an energy representation where

$$\hat{H}_{\text{band}} = \sum_{\sigma} \int d\varepsilon \varepsilon c_{\varepsilon\sigma}^{\dagger} c_{\varepsilon\sigma}, \quad (5)$$

$$\hat{H}_{\text{hyb}} = \sum_{\sigma} \int d\varepsilon \sqrt{\bar{\Gamma}(\varepsilon)/\pi} (\varepsilon c_{\varepsilon\sigma}^{\dagger} d_{\sigma} + \text{H.c.}), \quad (6)$$

shows that the conduction-band dispersion $\varepsilon_{\mathbf{k}}$ and the hybridization matrix element $V_{\mathbf{k}}$ affect the impurity degrees of freedom only in combination through the hybridization function [44]

$$\bar{\Gamma}(\varepsilon) \equiv \frac{\pi}{N_k} \sum_{\mathbf{k}} V_{\mathbf{k}}^2 \delta(\varepsilon - \varepsilon_{\mathbf{k}}). \quad (7)$$

To focus on the most interesting physics of the model, we assume a simplified form

$$\bar{\Gamma}(\varepsilon) = \Gamma |\varepsilon/D|^r \Theta(D - |\varepsilon|), \quad (8)$$

where $\Theta(x)$ is the Heaviside function and Γ is the hybridization width. The primary focus of this work is cases $r > 0$ in which the hybridization function exhibits a power-law pseudogap around the Fermi energy. We will also briefly discuss $r = 0$, representing a conventional metallic host.

One way that a hybridization function of the form of Eq. (8) can arise is from a purely local hybridization matrix element $V_{\mathbf{k}} = V \geq 0$ combined with a density of states (per unit cell, per spin orientation) varying as

$$\rho(\varepsilon) \equiv N_k^{-1} \sum_{\mathbf{k}} \delta(\varepsilon - \varepsilon_{\mathbf{k}}) = \rho_0 |\varepsilon/D|^r \Theta(D - |\varepsilon|) \quad (9)$$

with $\rho_0 = (1+r)/(2D)$, in which case $\Gamma = \pi\rho_0 V^2$. However, all results below apply equally to situations in which the \mathbf{k} dependence of the hybridization contributes to the energy dependence of $\bar{\Gamma}(\varepsilon)$.

The assumption that $\bar{\Gamma}(\varepsilon)$ exhibits a pure power-law dependence over the entire width of the conduction band is a convenient idealization. More realistic hybridization functions in which the power-law variation is restricted to a region around the Fermi energy exhibit the same qualitative physics, with modification only of nonuniversal properties such as the location of phase boundaries and the value of the Kondo temperature.

In the metallic ($r = 0$) Anderson model, any value $\Gamma > 0$ places the system in its strong-coupling phase, where the impurity degrees of freedom are completely quenched at $T = 0$. The situation for pseudogapped hybridization functions ($r > 0$) is much richer, as summarized in the phase diagrams shown in Fig. 1 for cases

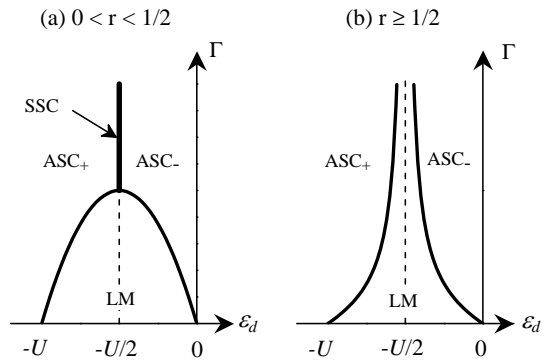


FIG. 1. Schematic ε_d - Γ phase diagrams of the pseudogap Anderson model [Eqs. (1)–(8)] for band exponents (a) $0 < r < \frac{1}{2}$, (b) $r \geq \frac{1}{2}$. Generically, the system falls into either a local-moment phase (LM) or one of two asymmetric strong-coupling phases (ASC_{\pm}). However, there is also a symmetric strong-coupling phase (the line labeled SSC) that is reached only for $0 < r < \frac{1}{2}$ under conditions of strict particle-hole symmetry ($\varepsilon_d = -\frac{1}{2}U$) and for sufficiently large hybridization widths Γ .

$U > 0$ of on-site Coulomb repulsion. The most notable feature is the existence within a region $-U < \varepsilon_d < 0$, $\Gamma < \Gamma_c(r, U, \varepsilon_d)$ of a local-moment (LM) phase within which the impurity retains an unquenched spin degree of freedom down to $T = 0$. There are also three different strong-coupling phases, distinguished by their ground-state electron number Q (measured from half filling): a symmetric strong-coupling (SSC) phase with $Q = 0$, reached only for $0 < r < \frac{1}{2}$ under the condition $\varepsilon_d = -\frac{1}{2}U$ for strict particle-hole (p - h) symmetry; and a pair of asymmetric strong-coupling phases ASC_+ and ASC_- having $Q = 1$ and $Q = -1$, respectively. The ranges $0 < r \leq \frac{1}{2}$ and $r \geq \frac{1}{2}$ can both be further subdivided based on the nature of the quantum phase transitions separating the phases. For a compact summary, the reader is referred to Sec. II B1 of Ref. 45.

B. Derivation of poor man's equations

This section presents a poor man's scaling treatment of the Anderson Hamiltonian with a power-law hybridization function. Jefferson [7] and Haldane [8] provided scaling treatments of the metallic case $r = 0$ valid in the limit $U \gg D$. These were subsequently extended to general values of U (Ref. 1), although the analysis neglected the renormalization of U . Reference 21 presented scaling equations for the pseudogap case $r > 0$ with $U = \infty$. Below, the scaling analysis is generalized to arbitrary values of r and U . Two of us have previously presented a similar poor man's scaling analysis of the Anderson-Holstein impurity model with a power-law hybridization [45]. The treatment of the Anderson model is somewhat simpler, and as we will see, the resulting scaling equa-

tions are amenable to approximate integration in several physically interesting limits.

We start with the Anderson Hamiltonian written in the form

$$\hat{H}'_A = \hat{H}_{\text{band}} + \hat{H}_{\text{imp}} + \hat{H}'_{\text{hyb}}, \quad (10)$$

where \hat{H}_{band} and \hat{H}_{imp} are as defined in Eqs. (2) and (3), respectively, but with \hat{H}_{hyb} in Eq. (4) replaced by

$$\begin{aligned} \hat{H}'_{\text{hyb}} = & \frac{1}{\sqrt{N_k}} \sum_{\mathbf{k}, \sigma} \{ [V_{0,\mathbf{k}}(1 - \hat{n}_{d,-\sigma}) \\ & + V_{1,\mathbf{k}} \hat{n}_{d,-\sigma}] d_{\sigma}^{\dagger} c_{\mathbf{k}\sigma} + \text{H.c.} \}, \end{aligned} \quad (11)$$

with hybridization functions

$$\bar{\Gamma}_{\tau}(\varepsilon) = \frac{\pi}{N_k} \sum_{\mathbf{k}} V_{\tau,\mathbf{k}}^2 \delta(\varepsilon - \varepsilon_{\mathbf{k}}) = \Gamma_{\tau} |\varepsilon/D|^r \Theta(D - |\varepsilon|) \quad (12)$$

for $\tau = 0, 1$ having the same power-law dependence as $\bar{\Gamma}(\varepsilon)$ defined in Eq. (8). At the bare Hamiltonian level, one expects the hybridization $V_{0,\mathbf{k}}$ between the empty and singly occupied impurity configurations to be identical to the matrix element $V_{1,\mathbf{k}}$ between the singly occupied and doubly occupied impurity configurations. However, this degeneracy might be broken under the scaling procedure.

Following Haldane [8], we focus on many-body states $|0\rangle$, $|\sigma\rangle = d_{\sigma}^{\dagger}|0\rangle$, and $|2\rangle = d_{\uparrow}^{\dagger}d_{\downarrow}^{\dagger}|0\rangle$ formed by combining the conduction-band ground state (having N_k electrons of energy $\varepsilon_{\mathbf{k}} < 0$) with one of the four possible configurations of the impurity level. Neglecting for the moment the effect of the hybridization (\hat{H}'_{hyb}), the energies of these states are denoted E_0 , $E_1 = \bar{E}_0 + \varepsilon_d$, and $E_2 = E_1 + \varepsilon_d + U = 2E_1 - E_0 + U$.

We now consider the effect of an infinitesimal reduction in the half-bandwidth from D to $\tilde{D} = D + dD$, where $dD < 0$. The goal is to write a new Hamiltonian \hat{H}'_A similar in form to \hat{H}'_A but retaining only conduction-band degrees of freedom having energies $|\varepsilon_{\mathbf{k}}| < \tilde{D}$ and with parameters $\tilde{\varepsilon}_d$, \tilde{U} , and $\tilde{V}_{\tau,\mathbf{k}}$ adjusted to account perturbatively for the band-edge states that have been eliminated.

Let K^+ be the set of wave vectors \mathbf{k} describing particle-like states having energies $\tilde{D} < \varepsilon_{\mathbf{k}} < D$, and K^- be the set of wave vectors describing hole-like state with energies $-D < \varepsilon_{\mathbf{k}} < -\tilde{D}$. Virtual tunneling of an electron from a K^- state into the empty impurity level transforms the state $|0\rangle$ to

$$|\tilde{0}\rangle = |0\rangle + \sum_{\sigma} \frac{1}{\sqrt{N_k}} \sum_{\mathbf{k} \in K^-} \frac{V_{0,\mathbf{k}}}{|\varepsilon_{\mathbf{k}}| + E_1 - E_0} c_{\mathbf{k}\sigma} |\sigma\rangle + O(V^2) \quad (13)$$

with energy

$$\begin{aligned} \tilde{E}_0 = & E_0 - \frac{2}{N_k} \sum_{\mathbf{k} \in K^-} \frac{V_{0,\mathbf{k}}^2}{|\varepsilon_{\mathbf{k}}| + E_1 - E_0} + O(V^3) \\ \simeq & E_0 - \frac{|dD|}{\pi} \frac{2\bar{\Gamma}_0(-D)}{D + \varepsilon_d} + O(V^3). \end{aligned} \quad (14)$$

Here, $O(V^n)$ schematically represents all processes involving a product of least n factors V_{τ_j,\mathbf{k}_j} . Similarly, virtual tunneling of an electron from the doubly occupied impurity level into a K^+ state transforms $|2\rangle$ to

$$|\tilde{2}\rangle = |2\rangle + \sum_{\sigma} \frac{\sigma}{\sqrt{N_k}} \sum_{\mathbf{k} \in K^+} \frac{V_{1,\mathbf{k}}}{\varepsilon_{\mathbf{k}} + E_1 - E_2} c_{\mathbf{k}\sigma}^{\dagger} |\sigma\rangle + O(V^2) \quad (15)$$

with energy

$$\begin{aligned} \tilde{E}_2 = & E_2 - \frac{2}{N_k} \sum_{\mathbf{k} \in K^+} \frac{V_{1,\mathbf{k}}^2}{\varepsilon_{\mathbf{k}} + E_1 - E_2} + O(V^3) \\ \simeq & E_2 - \frac{|dD|}{\pi} \frac{2\bar{\Gamma}_1(D)}{D - U - \varepsilon_d} + O(V^3). \end{aligned} \quad (16)$$

Finally, virtual tunneling of an electron into the singly occupied impurity from a K^- state or from the singly occupied level into a K^+ state transforms $|\sigma\rangle$ to

$$\begin{aligned} |\tilde{\sigma}\rangle = & |\sigma\rangle - \frac{\sigma}{\sqrt{N_k}} \sum_{\mathbf{k} \in K^-} \frac{V_{1,\mathbf{k}}}{|\varepsilon_{\mathbf{k}}| + E_2 - E_1} c_{\mathbf{k},-\sigma} |2\rangle \\ & - \frac{1}{\sqrt{N_k}} \sum_{\mathbf{k} \in K^+} \frac{V_{0,\mathbf{k}}}{\varepsilon_{\mathbf{k}} + E_0 - E_1} c_{\mathbf{k}\sigma}^{\dagger} |0\rangle + O(V^2) \end{aligned} \quad (17)$$

with energy

$$\begin{aligned} \tilde{E}_1 = & E_1 - \frac{1}{N_k} \sum_{\mathbf{k} \in K^-} \frac{V_{1,\mathbf{k}}^2}{|\varepsilon_{\mathbf{k}}| + E_2 - E_1} \\ & - \frac{1}{N_k} \sum_{\mathbf{k} \in K^+} \frac{V_{0,\mathbf{k}}^2}{\varepsilon_{\mathbf{k}} + E_0 - E_1} + O(V^3) \\ \simeq & E_1 - \frac{|dD|}{\pi} \left[\frac{\bar{\Gamma}_1(-D)}{D + U + \varepsilon_d} + \frac{\bar{\Gamma}_0(D)}{D - \varepsilon_d} \right] + O(V^3). \end{aligned} \quad (18)$$

The $O(V^2)$ terms in each of the above states $|\tilde{\phi}\rangle$ include ones required to enforce normalization, i.e., $\langle \tilde{\phi} | \tilde{\phi} \rangle = \langle \phi | \phi \rangle = 1$.

The modified energies can be used to define effective Hamiltonian parameters $\tilde{\varepsilon}_d = \tilde{E}_1 - \tilde{E}_0$ and $\tilde{U} = \tilde{E}_2 + \tilde{E}_0 - 2\tilde{E}_1$. At the same time, for each \mathbf{k} in the retained portion of the band (i.e., satisfying $|\varepsilon_{\mathbf{k}}| < \tilde{D}$), the hybridization matrix element $V_{0,\mathbf{k}}$ must be replaced by

$$\tilde{V}_{0,\mathbf{k}} = \begin{cases} \sqrt{N_k} \langle \tilde{0} | c_{\mathbf{k}\sigma} \hat{H}'_A | \tilde{\sigma} \rangle & \text{for } \varepsilon_{\mathbf{k}} > 0 \\ -\sqrt{N_k} \langle \tilde{\sigma} | c_{\mathbf{k}\sigma}^{\dagger} \hat{H}'_A | \tilde{0} \rangle & \text{for } \varepsilon_{\mathbf{k}} < 0, \end{cases} \quad (19)$$

and $V_{1,\mathbf{k}}$ must be replaced by

$$\tilde{V}_{1,\mathbf{k}} = \begin{cases} -\sigma\sqrt{N_k} \langle \tilde{\sigma} | c_{\mathbf{k},-\sigma} \hat{H}'_A | \tilde{2} \rangle & \text{for } \varepsilon_{\mathbf{k}} > 0 \\ \sigma\sqrt{N_k} \langle \tilde{2} | c_{\mathbf{k},-\sigma}^\dagger \hat{H}'_A | \tilde{\sigma} \rangle & \text{for } \varepsilon_{\mathbf{k}} < 0. \end{cases} \quad (20)$$

It is straightforward to show that

$$\tilde{V}_{\tau,\mathbf{k}} = V_{\tau,\mathbf{k}} + O(V^3). \quad (21)$$

The leading corrections to $\tilde{V}_{\tau,\mathbf{k}}$ involve numerous terms arising from the V^2 terms in the states $|\tilde{\phi}\rangle$. Since these corrections are too small to be of much practical importance, we shall not evaluate them here.

The infinitesimal band-edge reduction described in the previous paragraphs can be carried out repeatedly to reduce the half-bandwidth by a finite amount from D to $\tilde{D} < D$. Equations (14) and (18) indicate that during this process, the effective impurity level energy $\tilde{\varepsilon}_d = \tilde{E}_1 - \tilde{E}_0$ evolves according to the scaling equation

$$\frac{d\tilde{\varepsilon}_d}{d\tilde{D}} = \frac{1}{\pi} \left[\frac{\tilde{\Gamma}_{0,+}}{\tilde{D} - \tilde{\varepsilon}_d} - \frac{2\tilde{\Gamma}_{0,-}}{\tilde{D} + \tilde{\varepsilon}_d} + \frac{\tilde{\Gamma}_{1,-}}{\tilde{D} + \tilde{U} + \tilde{\varepsilon}_d} \right] + O(V^3), \quad (22)$$

where $\tilde{\Gamma}_{\tau,\pm}$ is the rescaled hybridization function at the reduced band edges $\varepsilon = \pm\tilde{D}$. Taking into account Eq. (16) as well, one sees that the effective on-site repulsion $\tilde{U} = \tilde{E}_2 + \tilde{E}_0 - 2\tilde{E}_1$ follows

$$\frac{d\tilde{U}}{d\tilde{D}} = \frac{2}{\pi} \left[\frac{\tilde{\Gamma}_{0,-}}{\tilde{D} + \tilde{\varepsilon}_d} - \frac{\tilde{\Gamma}_{0,+}}{\tilde{D} - \tilde{\varepsilon}_d} + \frac{\tilde{\Gamma}_{1,+}}{\tilde{D} - \tilde{U} - \tilde{\varepsilon}_d} - \frac{\tilde{\Gamma}_{1,-}}{\tilde{D} + \tilde{U} + \tilde{\varepsilon}_d} \right] + O(V^3). \quad (23)$$

The band-edge values $\tilde{\Gamma}_{\tau,\pm}$ of the hybridization functions $\tilde{\Gamma}_\tau(\varepsilon)$ rescale both due to the replacement of D by \tilde{D} in Eq. (8) and due to the perturbative corrections to $V_{\tau,\mathbf{k}}$ in Eq. (21), leading to the scaling equation

$$\frac{d\tilde{\Gamma}_{\tau,\pm}}{d\tilde{D}} = r \frac{\tilde{\Gamma}_{\tau,\pm}}{\tilde{D}} + O(V^4). \quad (24)$$

The scaling equations (22)–(24) have been derived to lowest order in nondegenerate perturbation theory, and are strictly valid only so long as $|\tilde{D} \pm (\tilde{\varepsilon}_d + \tau U)| \gg \tilde{V}_{\tau,\mathbf{k}}$ for each \mathbf{k} such that $\varepsilon_{\mathbf{k}} = \mp\tilde{D}$.

Equation (24) shows that the band-edge values of the hybridization functions $\tilde{\Gamma}_\tau(\varepsilon)$ are irrelevant (in the RG sense) for $r > 0$ and at most marginally relevant for $r = 0$. For the p - h -symmetric bare hybridization functions considered in this work, it is an excellent approximation to set $\tilde{\Gamma}_{0,\pm} = \tilde{\Gamma}_{1,\pm} = \tilde{\Gamma}$, leading to the simplified scaling

equations

$$\frac{d\tilde{\Gamma}}{d\tilde{D}} = r \frac{\tilde{\Gamma}}{\tilde{D}}, \quad (25)$$

$$\frac{d\tilde{\varepsilon}_d}{d\tilde{D}} \simeq \frac{\tilde{\Gamma}}{\pi} \left[\frac{1}{\tilde{D} - \tilde{\varepsilon}_d} - \frac{2}{\tilde{D} + \tilde{\varepsilon}_d} + \frac{1}{\tilde{D} + \tilde{U} + \tilde{\varepsilon}_d} \right], \quad (26)$$

$$\frac{d\tilde{U}}{d\tilde{D}} \simeq \frac{2\tilde{\Gamma}}{\pi} \left[\frac{1}{\tilde{D} + \tilde{\varepsilon}_d} - \frac{1}{\tilde{D} - \tilde{\varepsilon}_d} + \frac{1}{\tilde{D} - \tilde{U} - \tilde{\varepsilon}_d} - \frac{1}{\tilde{D} + \tilde{U} + \tilde{\varepsilon}_d} \right]. \quad (27)$$

Equations (25)–(27) with initial conditions $\tilde{\varepsilon}_d = \varepsilon_d$, $\tilde{U} = U$, and $\tilde{\Gamma} = \Gamma$ represent the main results of this section. The equations respect p - h symmetry in that

$$\frac{d(\tilde{\varepsilon}_d + \frac{1}{2}\tilde{U})}{d\tilde{D}} \simeq \frac{2\tilde{\Gamma}}{\pi} \frac{\tilde{\varepsilon}_d + \frac{1}{2}\tilde{U}}{(\tilde{D} - \frac{1}{2}\tilde{U})^2 - (\tilde{\varepsilon}_d + \frac{1}{2}\tilde{U})^2}, \quad (28)$$

so bare couplings satisfying $\varepsilon_d = -\frac{1}{2}U$ inevitably lead to rescaled couplings that satisfy $\tilde{\varepsilon}_d = -\frac{1}{2}\tilde{U}$. For $r = 0$, Eqs. (25)–(27) reproduce the scaling equations for the metallic Anderson problem [1], while for $r > 0$ in the limit $U \rightarrow \infty$ of extreme p - h asymmetry, Eqs. (25) and (26) reduce to ones presented previously [21] for pseudogapped systems.

Equation (25) clearly has the solution

$$\tilde{\Gamma} = (\tilde{D}/D)^r \Gamma. \quad (29)$$

Substituting this expression for $\tilde{\Gamma}$ into Eqs. (26) and (27) creates a pair of coupled differential equations for $\tilde{\varepsilon}_d$ and \tilde{U} . Analytical or numerical integration of these differential equations allows one to follow the evolution of the rescaled couplings under reduction of \tilde{D} until one of the following conditions is met, signaling entry into a low-energy regime governed by a simpler effective model than the full pseudogap Anderson model:

(1) If $\tilde{\varepsilon}_d, \tilde{U} + 2\tilde{\varepsilon}_d > \tilde{D} > \tilde{\Gamma}$, the system lies in the empty-impurity region of the ASC_- strong-coupling phase, in which the ground-state impurity occupancy approaches zero. In this case, $T^* = \min(\tilde{\varepsilon}_d, \tilde{U} + 2\tilde{\varepsilon}_d)$ sets the scale for crossover into a low-energy regime of (for $r > 0$, generalized) Fermi-liquid behavior.

(2) If $-(\tilde{U} + \tilde{\varepsilon}_d), -(\tilde{U} + 2\tilde{\varepsilon}_d) > \tilde{D} > \tilde{\Gamma}$, the system belongs in the full-impurity region of the ASC_+ strong-coupling phase, in which the ground-state impurity occupancy approaches two. Here, $T^* = \min(-(\tilde{U} + \tilde{\varepsilon}_d), -(\tilde{U} + 2\tilde{\varepsilon}_d))$ marks crossover into the asymptotic (generalized) Fermi-liquid regime.

(3) If $-\tilde{\varepsilon}_d, \tilde{U} + \tilde{\varepsilon}_d > \tilde{D} > \tilde{\Gamma}$, the system crosses over into an intermediate-energy regime of local-moment behavior. (This *regime* is distinct from the LM *phase*, which is defined by its ground-state properties.) On entry to the LM regime, the empty and doubly occupied impurity configurations are effectively frozen out, and one can perform a generalization [31] of the Schrieffer-Wolff transformation [46] to map the pseudogap Anderson model to

a pseudogap Kondo model

$$H_K = H_{\text{band}} + \frac{1}{N_k} \sum_{\mathbf{k}, \mathbf{k}'} \sum_{\sigma, \sigma'} c_{\mathbf{k}\sigma}^\dagger \left[\frac{J}{2} \hat{\mathbf{S}} \cdot \boldsymbol{\sigma}_{\sigma\sigma'} + K \delta_{\sigma, \sigma'} \right] c_{\mathbf{k}'\sigma'} \quad (30)$$

where \hat{H}_{band} is as given in Eq. (2) with the power-law density of states specified in Eq. (9), $\hat{\mathbf{S}}$ is the spin- $\frac{1}{2}$ operator for the impurity, $\boldsymbol{\sigma}$ is a vector of Pauli matrices, the (isotropic) exchange coupling J satisfies

$$\rho_0 J = \frac{2\tilde{\Gamma}}{\pi} \left(\frac{1}{|\tilde{\varepsilon}_d|} + \frac{1}{\tilde{U} + \tilde{\varepsilon}_d} \right), \quad (31)$$

and the potential scattering K satisfies

$$\rho_0 K = \frac{\tilde{\Gamma}}{2\pi} \left(\frac{1}{|\tilde{\varepsilon}_d|} - \frac{1}{\tilde{U} + \tilde{\varepsilon}_d} \right). \quad (32)$$

For metallic hosts ($r = 0$), a system that reaches the LM regime always lies in the strong-coupling phase of the Kondo model, which constitutes another region of the strong-coupling phase of the Anderson model. In pseudogap cases, by contrast, the asymptotic low-energy behavior depends on the values of J and K : the system may fall in one of three Kondo phases that are associated with the SSC (for $K = 0$), ASC_- (for $K > 0$), or ASC_+ (for $K < 0$) phases of the Anderson model; or it may fall in the LM phase of both the Kondo and Anderson models, in which the impurity retains a free two-fold spin degree of freedom down to absolute zero. In any of these cases, the energy scale T^* for crossover into the asymptotic low-energy regime is generally much smaller than the scale $\min(-\tilde{\varepsilon}_d, \tilde{U} + \tilde{\varepsilon}_d)$ for entry into the LM regime. On approach to a strong-coupling ground state, T^* coincides with the Kondo temperature T_K .

(4) If $\tilde{\varepsilon}_d, -(\tilde{U} + \tilde{\varepsilon}_d) > \tilde{D} > \tilde{\Gamma}, \tilde{U} + 2\tilde{\varepsilon}_d$ (a situation that arises only if the bare U is negative), then the system enters the intermediate-energy local-charge regime. At this point, one can perform a generalized Schrieffer-Wolff transformation to a pseudogap charge-Kondo model. The system may lie in a strong-coupling phase of the charge-Kondo model (yet another region of an Anderson-model strong-coupling phase) or in the local-charge phase of both models, where the impurity retains a free two-fold charge degree of freedom down to absolute zero. Similarly to the situation in (3), the crossover to the asymptotic low-energy regime is characterized by a scale $T^* \ll \min(\tilde{\varepsilon}_d, -(\tilde{U} + \tilde{\varepsilon}_d))$.

(5) If $\tilde{\Gamma} > \tilde{D} > |\tilde{\varepsilon}_d|$ and/or $\tilde{\Gamma} > \tilde{D} > |\tilde{U} + \tilde{\varepsilon}_d|$, then the system enters a mixed-valence regime where the states $|\hat{0}\rangle$, $|\hat{\sigma}\rangle$, and $|\hat{2}\rangle$ are no longer all well-defined. The scaling method is unable to determine whether the system lies in the mixed-valence region of the strong-coupling phase, or instead falls in the local-moment or local-charge phase [47].

In the remainder of Sec. II, we specialize to ranges of the band exponent $r > 0$ and the bare parameters

U (henceforth taken to be positive, representing on-site Coulomb repulsion), ε_d , and Γ for which it possible to make analytical predictions for the location of boundaries between LM and strong-coupling phases. We compare these predictions with results obtained using the non-perturbative numerical renormalization group (NRG) method [48, 49], as adapted to treat systems containing a pseudogap density of states [30, 31]. Throughout the paper, we have set Wilson's discretization parameter to $\Lambda = 3$ and kept up to 600 many-body states after each iteration of the NRG.

C. Phase boundaries for $r > 1$

Analysis of band exponents in the range $r > 1$ is simplified because Eq. (29) means that $\tilde{\Gamma}/\tilde{D} = (\tilde{D}/D)^{r-1}(\Gamma/D)$ decreases monotonically under reduction of the half-bandwidth. In the physically most relevant range $\Gamma < D$, this decrease in $\tilde{\Gamma}/\tilde{D}$ rules out the possibility of entry into the mixed-valence regime under condition (5) of Sec. II B. Moreover, the decrease of $\tilde{\Gamma}$ is so rapid that any entry to the local-moment regime and subsequent mapping to the pseudogap Kondo problem [via Eqs. (31) and (32)] will yield a sub-critical exchange coupling that assigns the system to the local-moment phase [31].

Under these circumstances, the upper critical level energy $\varepsilon_{d,c}^+(\Gamma, U)$ separating the ASC_- phase (in which $\tilde{\varepsilon}_d = \tilde{D}$ is satisfied at sufficiently low \tilde{D}) from the LM phase (in which one eventually reaches $\tilde{\varepsilon}_d = -\tilde{D}$) is effectively determined by the condition $\tilde{\varepsilon}_d(\tilde{D} = 0) = 0$ that places the fully renormalized impurity level precisely at the the Fermi energy. This picture of the quantum phase transition as arising from a renormalized level crossing is consistent with the observation of first-order behavior for $r > 1$ [33, 38]. By p - h symmetry, the boundary between the LM and ASC_+ phases is at the lower critical level energy $\varepsilon_{d,c}^- = -U - \varepsilon_{d,c}^+$ [see Fig. 1(b)].

The aforementioned boundary between the LM and ASC_- phases can be located by performing an approximate integration of Eqs. (26) and (27) using Eq. (29). For uniformity of presentation, we express our result in the form of a critical hybridization width $\Gamma_c(U, \varepsilon_d)$. We will consider bare parameters satisfying $0 < -\varepsilon_d \ll U + \varepsilon_d$, D and (for reasons that will become clear shortly) $\Gamma \ll (r-1)D$. Cases $U \ll D$ and $U \gg D$ will be considered separately.

1. LM- ASC_- boundary for $0 < -\varepsilon_d \ll U$ and $\Gamma, U \ll D$

If $U \ll D$, then so long as $|\tilde{\varepsilon}_d|, \tilde{U} + \tilde{\varepsilon}_d \ll \tilde{D}$, Eq. (27) can be approximated by

$$\frac{d\tilde{U}}{d\tilde{D}} \simeq \frac{4\tilde{\Gamma}\tilde{U}}{\pi\tilde{D}^2} = \frac{4\Gamma}{\pi D^r} \tilde{U}\tilde{D}^{r-2}, \quad (33)$$

where use has been made of Eq. (29). This differential equation can be integrated to yield

$$\tilde{U}(\tilde{D}) \simeq U \exp \left[-\frac{4}{(r-1)\pi} \left(\frac{\Gamma}{\tilde{D}} - \frac{\tilde{\Gamma}}{\tilde{D}} \right) \right], \quad (34)$$

which for $\Gamma/\tilde{D} \ll (r-1)\pi$ describes a very weak downward renormalization of \tilde{U} with decreasing \tilde{D} .

During the same initial phase of the scaling, Eq. (28) can be approximated by

$$\frac{d}{d\tilde{D}}(\tilde{\varepsilon}_d + \frac{1}{2}\tilde{U}) \simeq \frac{2\Gamma}{\pi D^r} (\tilde{\varepsilon}_d + \frac{1}{2}\tilde{U})\tilde{D}^{r-2}, \quad (35)$$

and hence

$$\tilde{\varepsilon}_d + \frac{1}{2}\tilde{U} \simeq (\varepsilon_d + \frac{1}{2}U) \exp \left[-\frac{2}{(r-1)\pi} \left(\frac{\Gamma}{\tilde{D}} - \frac{\tilde{\Gamma}}{\tilde{D}} \right) \right]. \quad (36)$$

Equations (34) and (36) imply that

$$\tilde{\varepsilon}_d - \varepsilon_d \simeq \frac{1}{4} \left(1 - \frac{2\varepsilon_d}{U} \right) (U - \tilde{U}). \quad (37)$$

In the case of present interest where $|\varepsilon_d| \ll U$, the level energy scales upward in absolute terms by one-quarter the amount that the on-site interaction scales down, but ε_d experiences a much greater fractional shift than U .

Equations (33), (34), and (36) remain valid until $(\tilde{U} + \tilde{\varepsilon}_d)/\tilde{D}$ rises to approach unity, a condition that occurs [for the assumed ordering of the bare parameters, and for the weak renormalization of U that holds for $\Gamma \ll (r-1)D$] at $\tilde{D} = \tilde{D}_1 \simeq U$, at which point

$$\tilde{\varepsilon}_{d,1} \equiv \tilde{\varepsilon}_d(\tilde{D}_1) \simeq \varepsilon_d + \frac{\Gamma U [1 - (U/D)^{r-1}]}{(r-1)\pi D}. \quad (38)$$

In the regime $\tilde{D} < \tilde{D}_1$, the doubly occupied impurity configuration is essentially frozen out. Now Eq. (26) can be approximated by

$$\frac{d\tilde{\varepsilon}_d}{d\tilde{D}} \simeq -\frac{\tilde{\Gamma}(\tilde{D} - 3\tilde{\varepsilon}_d)}{\pi\tilde{D}^2} = -\frac{\Gamma}{\pi D^r} (\tilde{D} - 3\tilde{\varepsilon}_d)\tilde{D}^{r-2}, \quad (39)$$

which has the solution

$$\tilde{\varepsilon}_d \simeq \tilde{\varepsilon}_{d,1} + \frac{\Gamma}{r\pi} \left[\left(\frac{\tilde{D}_1}{\tilde{D}} \right)^r - \left(\frac{\tilde{D}}{\tilde{D}_1} \right)^r \right] \left[1 + O\left(\frac{\tilde{\varepsilon}_{d,1}}{U} \right) \right]. \quad (40)$$

Using Eq. (38), this gives

$$\tilde{\varepsilon}_d(\tilde{D}) \simeq \varepsilon_d + \frac{\Gamma}{(r-1)\pi} \left[\frac{U}{\tilde{D}} - \frac{1}{r} \left(\frac{U}{\tilde{D}} \right)^r - \frac{r-1}{r} \left(\frac{\tilde{D}}{\tilde{D}_1} \right)^r \right]. \quad (41)$$

A more careful treatment of scaling over the range of \tilde{D} in which $|\tilde{D} - \tilde{U} - \tilde{\varepsilon}_d| \lesssim \tilde{\Gamma}$ [invalidating the nondegenerate perturbation theory used to derive Eqs. (25)–(27)] would likely modify the numerical prefactor of $(U/\tilde{D})^r \Gamma$ on the right-hand side of Eq. (41). With this caveat, the

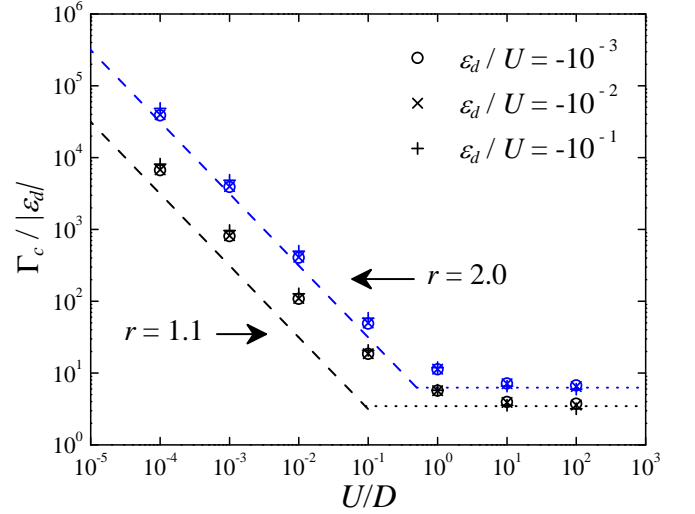


FIG. 2. Critical hybridization width plotted as $\Gamma_c/|\varepsilon_d|$ vs U/D , comparing NRG data (symbols) with the scaling predictions of Eq. (43) (dashed lines) and Eq. (45) (dotted lines). Results are for $r = 1.1$ and 2 and for three values of $|\varepsilon_d|/U$ shown in the legend.

equation should capture the scaling of the impurity level energy until $|\tilde{\varepsilon}_d|/\tilde{D}$ grows to reach 1 at some reduced half-bandwidth \tilde{D}_2 . For $\tilde{D} < \tilde{D}_2$, the system crosses over into the low-energy regime of the ASC_- phase (for $\tilde{\varepsilon}_d > 0$) or that of the LM phase (for $\tilde{\varepsilon}_d < 0$). The only exception occurs for a combination of bare parameters that places the system precisely on the boundary between the two phases, in which case $\tilde{\varepsilon}_d(\tilde{D} = 0) = 0$. Recalling that we are considering cases $r > 1$, Eq. (41) shows that the boundary location $\varepsilon_{d,c}^+(U, \Gamma)$ is primarily determined by initial phase of scaling ($\tilde{D}_1 < \tilde{D} < D$), and to leading order in U/D and Γ/D satisfies

$$\varepsilon_{d,c}^+ \simeq -\frac{\Gamma U}{(r-1)\pi D}. \quad (42)$$

This relation can be recast as

$$\Gamma_c \simeq (r-1)\pi D |\varepsilon_d|/U \quad (43)$$

for $-U/2 \ll \varepsilon_d < 0$.

The phase boundary between the LM and ASC_- phases at $\Gamma_c(U, \varepsilon_d)$ can be determined to the desired accuracy by performing successive NRG runs to refine the value of Γ_c using the method of bisection. At the end of each run, the zero-temperature limit of $T\chi_{\text{imp}}$ (temperature times the impurity contribution to the static magnetic susceptibility) [50, 51] is used to determine whether the system is in the LM phase ($T\chi_{\text{imp}} \rightarrow 1/4$) or in the ASC_- phase ($T\chi_{\text{imp}} \rightarrow 0$), and thus to modify the range of Γ values within which Γ_c must lie.

Figure 2 shows the critical hybridization width plotted as $\Gamma_c(U, \varepsilon_d)/|\varepsilon_d|$ vs U/D for $r = 1.1$ and 2 . NRG results (symbols) calculated for three different fixed ratios

$-\frac{1}{2} \ll \varepsilon_d/U < 0$ are compared with the scaling expression in Eq. (43) (dashed lines). The numerics confirm the predicted linear dependence of Γ_c on ε_d . The U^{-1} variation of Γ_c is also well supported for $r = 2$, but for $r = 1.1$ is only approached in the limit of very small U/D . This deviation from the scaling theory likely arises because the latter band exponent lies close to the value $r = 1$ that acts as an upper critical dimension for the pseudogap Anderson and Kondo models and at which there are logarithmic corrections to simple power-law behaviors [25, 33, 38]. Results for $1.1 < r < 2$ (not shown) indicate that increasing r leads to a continuous improvement in the accuracy with which Eq. (43) reproduces the NRG data.

2. LM-ASC₋ boundary for $0 < -\varepsilon_d, \Gamma \ll D \ll U$

If the bare parameters of the Anderson Hamiltonian instead satisfy $U \gg D$, then Eq. (39) applies from the outset of scaling, and $\tilde{\varepsilon}_d$ satisfies Eq. (40) with $\tilde{D}_1 = D$ and $\tilde{\varepsilon}_{d,1} = \varepsilon_d$, i.e.,

$$\tilde{\varepsilon}_d(\tilde{D}) \simeq \varepsilon_d + \frac{\Gamma}{r\pi} \left[1 - \left(\frac{\tilde{D}}{D} \right)^r \right]. \quad (44)$$

Now the condition $\tilde{\varepsilon}_d(\tilde{D} = 0) = 0$ places the LM-ASC₋ phase boundary at

$$\Gamma_c \simeq r\pi|\varepsilon_d|. \quad (45)$$

Figure 2 compares the prediction of Eq. (45) (dotted lines) with NRG results obtained for $U \geq D$. The scaling approach reproduces the numerical results very well for $U \gtrsim 10D$, and (in contrast to the behavior found for $U \ll D$) there is no significant difference between $r = 1.1$ and $r = 2$ in the accuracy of the analytical results.

D. Phase boundaries for $0 < r < 1$

For $r < 1$, Eq. (29) implies that $\tilde{\Gamma}/\tilde{D} = (D/\tilde{D})^{1-r}(\Gamma/D) \geq \Gamma/D$. The system flows to mixed valence [under condition (5) in Sec. II B] at a reduced half-bandwidth

$$\tilde{D}_\Gamma = \tilde{\Gamma}(\tilde{D}_\Gamma) = (\Gamma/D)^{1/(1-r)} D \quad (46)$$

provided that $|\tilde{\varepsilon}_d(\tilde{D}_\Gamma)|$ and $|\tilde{U}(\tilde{D}_\Gamma) + \tilde{\varepsilon}_d(\tilde{D}_\Gamma)|$ both remain smaller than \tilde{D}_Γ . However, the system flows to a different low-energy regime if $|\tilde{\varepsilon}_d/\tilde{D}$ or $|\tilde{U} + \tilde{\varepsilon}_d|/\tilde{D}$ reaches 1 at some $\tilde{D} > \tilde{D}_\Gamma$.

1. LM-SSC boundary for $\Gamma, U \ll D$

We first consider cases $\varepsilon_d = -\frac{1}{2}U$ where the system exhibits strict p - h symmetry, and focus on the universal (large-bandwidth) limit $\Gamma, U \ll D$.

So long as $\frac{1}{2}\tilde{U} \ll \tilde{D}$, Eq. (27) can again be approximated by Eq. (33), which can be integrated to yield

$$\tilde{U}(\tilde{D}) \simeq U \exp \left[-\frac{4}{(1-r)\pi} \left(\frac{\tilde{\Gamma}}{\tilde{D}} - \frac{\Gamma}{D} \right) \right]. \quad (47)$$

Equation (47) can be reexpressed as

$$(\tilde{U}/2\tilde{D})^{1-r} \simeq \tilde{x} e^{-\gamma \tilde{x}} \quad (48)$$

in terms of new variables

$$\tilde{x}(\tilde{D}) = \left(\frac{U}{2\tilde{D}} \right)^{1-r} \exp \left(\frac{4\Gamma}{\pi\tilde{D}} \right) \geq x \equiv \tilde{x}(D) \quad (49)$$

and

$$\gamma = \left(\frac{2D}{U} \right)^{1-r} \left(\frac{4\Gamma}{\pi D} \right) \exp \left(-\frac{4\Gamma}{\pi D} \right) \quad (50)$$

that allow Eq. (29) to be recast exactly in the form

$$\tilde{\Gamma}/\tilde{D} = \frac{\pi}{4} \gamma \tilde{x}. \quad (51)$$

Equation (48) shows that with increasing \tilde{x} (or decreasing \tilde{D}), $\tilde{U}/2\tilde{D}$ initially rises, before peaking at $\tilde{x} = 1/\gamma$, and then dropping off exponentially for $\tilde{x} \gg 1/\gamma$. The system will enter its local-moment regime [under condition (3) in Sec. II B] if there exists a reduced half-bandwidth $\tilde{D}_U > \tilde{D}_\Gamma$ such that $\tilde{U}(\tilde{D}_U)/2\tilde{D}_U = 1$. The approximate scaling equation (33) is valid only so long as $\tilde{U}/\tilde{D} \lesssim 1$. Equation (27) predicts that \tilde{U} experiences a stronger downward renormalization once \tilde{U}/\tilde{D} approaches 2, a range in which the nondegenerate perturbation theory used to derive Eqs. (25)–(27) also begins to break down. However, in this range of $\tilde{U}/2\tilde{D}$, physically one expects renormalization to slow to a halt as charge fluctuations are progressively frozen out. Therefore, in the spirit of Haldane [8], we apply Eq. (48) all the way to the point where $\tilde{U}(\tilde{D})/2\tilde{D} = 1$, and we seek \tilde{x}_U defined to be the smallest solution of

$$\tilde{x} e^{-\gamma \tilde{x}} = 1. \quad (52)$$

For $\gamma > 1/e$, Eq. (52) has no real solution, so the system necessarily crosses over to mixed valence for $\tilde{D} \lesssim \tilde{D}_\Gamma$. For $0 \leq \gamma \leq 1/e$, by contrast, Eq. (52) has a solution $\tilde{x}_U(\gamma)$ satisfying $1 \leq \tilde{x}_U \leq e \leq \gamma^{-1}$. Since $\gamma \tilde{x}_U < 1$, Eq. (51) gives $\tilde{\Gamma}(\tilde{D}_U) < \tilde{D}_U$, meaning that at $\tilde{D} = \tilde{D}_U$ the system satisfies condition (3) for crossover into its local-moment regime. Equation (49) gives

$$\frac{\tilde{U}}{U} = \frac{2\tilde{D}_U}{U} = \left[\frac{\exp(4\Gamma/\pi D)}{\tilde{x}_U(\gamma)} \right]^{1/(1-r)} \geq e^{-1/(1-r)} \quad (53)$$

since $\tilde{x}_U \leq e$. This implies, at least for $r \ll \frac{1}{2}$, that the rescaled on-site interaction $\tilde{U}(\tilde{D}_U)$ remains of the same order as U .

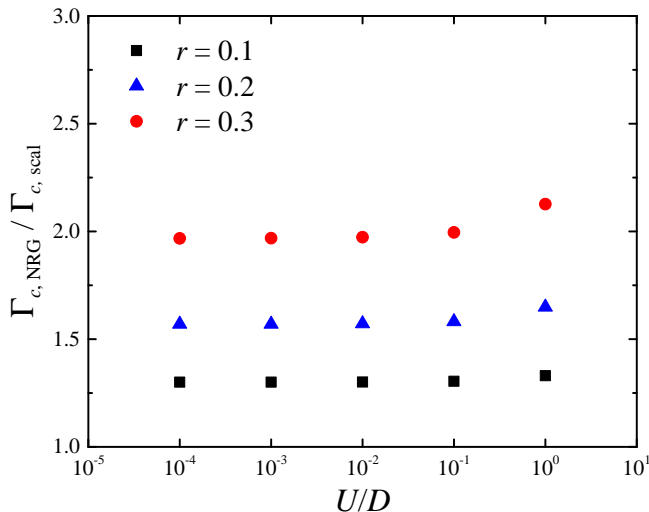


FIG. 3. Ratio $\Gamma_{c,\text{NRG}}/\Gamma_{c,\text{scal}}$ of the critical hybridization width found using NRG to the scaling prediction given by Eq. (56), plotted as a function of U/D for $\varepsilon_d = -U/2$ and band exponents $r = 0.1, 0.2$, and 0.3 .

A Schrieffer-Wolff transformation performed at $\tilde{D} = \tilde{D}_U$ yields a pseudogap Kondo model with [Eqs. (31) and (32)]

$$\rho_0 J = \frac{8\tilde{\Gamma}(\tilde{D}_U)}{\pi\tilde{U}(\tilde{D}_U)} = \gamma \tilde{x}_U, \quad \rho_0 K = 0. \quad (54)$$

It is known that for $\rho_0 K = 0$, the critical exchange coupling J_c separating the Kondo ($J > J_c$) and LM ($J < J_c$) phases satisfies $\rho_0 J_c = f(r)$ where $f(r) \simeq r(1+r/2)$ for $r \ll \frac{1}{2}$ (Refs. 19 and 20) and $f(r) \rightarrow \infty$ for $r \rightarrow \frac{1}{2}^-$ (Ref. 29). Combining this information with Eq. (54), one arrives at the prediction that the boundary between the LM and SSC phases is determined by the condition $\gamma_c \tilde{x}_U(\gamma_c) = f(r)$. Then, Eq. (52) gives $\tilde{x}_c \equiv \tilde{x}_U(\gamma_c) = \exp[f(r)]$ and, hence, $\gamma_c = f(r)/\tilde{x}_c = f(r) \exp[-f(r)]$. This means that the LM phase occupies the parameter range $U > U_c(\Gamma)$, where

$$U_c = 2D \left\{ \frac{\exp[f(r)]}{f(r)} \frac{4\Gamma}{\pi D} \exp\left(-\frac{4\Gamma}{\pi D}\right) \right\}^{1/(1-r)}. \quad (55)$$

For $\Gamma \ll D$, one can invert Eq. (55) to deduce that the LM phase occupies the parameter range $\Gamma < \Gamma_c(U)$, with

$$\Gamma_c \simeq D \frac{\pi f(r)}{4 \exp[f(r)]} \left(\frac{U}{2D} \right)^{1-r}. \quad (56)$$

A U^{1-r} variation of Γ_c was found previously using the local-moment approach [39], which yields a closed-form expression for $r \rightarrow 0^+$ that is identical to the corresponding limit of Eq. (56).

Figure 3 plots the ratio of the critical hybridization width $\Gamma_{c,\text{NRG}}$ found using the NRG to the scaling prediction $\Gamma_{c,\text{scal}}$ given by Eq. (56). For band exponents

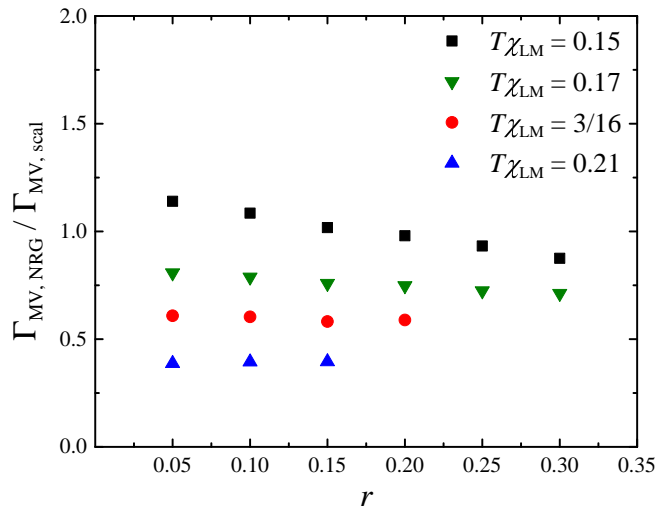


FIG. 4. Ratio $\Gamma_{\text{MV,NRG}}/\Gamma_{\text{MV,scal}}$ of the mixed-valence threshold hybridization width found using NRG and that given by poor man's scaling. Results for fixed $U = -2\varepsilon_d = 10^{-4}D$ are plotted vs band exponent r with $\Gamma_{\text{MV,NRG}}$ defined using four different values of $T\chi_{\text{LM}}$ (see text for details). For $T\chi_{\text{LM}} = 3/16$ [0.21], it proves impossible to find Kondo-region behavior for $r \geq 0.2$ [$r \geq 0.15$].

$r = 0.1, 0.2$, and 0.3 , this ratio is well converged for $U/D \lesssim 0.1$, implying that the scaling analysis correctly captures the U^{1-r} dependence of Γ_c at the LM-SSC phase boundary. The absolute value of $\Gamma_{c,\text{NRG}}/\Gamma_{c,\text{scal}}$ falls as r decreases, and seems likely to approach unity as $r \rightarrow 0^+$. We infer that Eq. (56) describes the NRG results apart from a multiplicative correction factor that depends solely on the band exponent r .

2. Kondo-mixed valence crossover for $\Gamma, U \ll D$

Poor man's scaling not only can find the LM-SSC phase boundary at $\Gamma = \Gamma_c$, but also can locate a crossover within the SSC phase at $\Gamma = \Gamma_{\text{MV}}$ between a Kondo region, in which only the singly occupied impurity configurations have significant occupation at low temperatures, and a mixed-valence region also having significant ground-state occupancy of the empty and/or doubly occupied impurity configuration(s). We have seen [after Eq. (52)] that the system reaches mixed valence for $\gamma > e^{-1}$ (equivalent to $\Gamma > \Gamma_{\text{MV}}$, a mixed-valence threshold hybridization), and argued [before Eq. (55)] that it enters the LM phase for $\gamma < \gamma_c = f(r) \exp[-f(r)]$. Therefore, the system exhibits fully developed Kondo physics (i.e., enters its local-moment regime at intermediate values of \tilde{D} and then crosses over to the SSC ground state for $\tilde{D} \lesssim T_K$) only for $\gamma_c < \gamma \leq e^{-1}$, equivalent to the condition $\Gamma_c < \Gamma \leq \Gamma_{\text{MV}}$ with

$$\Gamma_{\text{MV}} \simeq \Gamma_c \exp[f(r) - 1]/f(r). \quad (57)$$

The Kondo region has a width $\Delta\Gamma = \Gamma_{\text{MV}} - \Gamma_c$ that narrows rapidly with increasing r and turns out to be restricted to $\Delta\Gamma \lesssim \Gamma_c/4$ for $r \gtrsim \frac{1}{3}$. For band exponents in the range $\frac{1}{3} \lesssim r < \frac{1}{2}$, the SSC phase can be accessed only from mixed valence, while for $r \geq \frac{1}{2}$ this phase disappears altogether [30, 31].

Within the NRG approach, we can define the mixed-valence threshold hybridization width by examining the temperature dependence of the impurity contribution to the magnetic susceptibility χ_{imp} . We can identify the Anderson model as being in its local-moment regime if $T\chi_{\text{imp}} > T\chi_{\text{LM}}$ where $T\chi_{\text{LM}}$ is a (somewhat arbitrary) cutoff chosen to lie between the value $T\chi_{\text{imp}} = 1/4$ corresponding to a free spin- $\frac{1}{2}$ degree of freedom and the high-temperature or mixed-valent limiting value $T\chi_{\text{imp}} = 1/8$. With this criterion, the system is in the Kondo region of the SSC phase if with decreasing T , $T\chi_{\text{imp}}$ first rises above $T\chi_{\text{LM}}$ before dropping towards its SSC value [31] of $r/8$. We therefore define $\Gamma_{\text{MV,NRG}}$ as the smallest hybridization width Γ for which $T\chi_{\text{imp}} < T\chi_{\text{LM}}$ at all temperatures.

Figure 4 shows the ratio $\Gamma_{\text{MV,NRG}}/\Gamma_{\text{MV,scal}}$ between the mixed-valence threshold coupling found using NRG and the scaling prediction of Eq. (57). The ratio is plotted vs band exponent r for fixed $U/D = 10^{-4}$ and four different cutoffs: $T\chi_{\text{LM}} = 0.15, 0.17, 3/16$, and 0.21. As one would expect, increasing the value of $T\chi_{\text{LM}}$ creates a more stringent criterion for the identification of Kondo physics, reduces the range of exponents r over which Kondo-region behavior is found, and for given r reduces the value of Γ_{MV} . However, the ratio $\Gamma_{\text{MV,NRG}}/\Gamma_{\text{MV,scal}}$ is nearly independent of r except in the case $T\chi_{\text{LM}} = 0.15$. This confirms that the condition for reaching mixed valence is correctly captured by Eq. (57) apart from a multiplicative factor that depends on the value of the cutoff $T\chi_{\text{LM}}$.

3. LM-ASC₋ boundary for $0 < -\varepsilon_d \ll U + \varepsilon_d$ and $\Gamma \ll D$

We now turn to the limit $0 < -\varepsilon_d \ll U + \varepsilon_d$, D of strong p - h asymmetry on the impurity site. In order to locate the boundary between the LM and ASC₋ phases, we will perform an approximate integration of Eqs. (26) and (27) using Eq. (29). We first consider $\Gamma, U \ll D$. The situation where $\Gamma \ll D \ll U$ will be considered at the end of the section.

So long as $|\tilde{\varepsilon}_d|, \tilde{U} + \tilde{\varepsilon}_d \ll \tilde{D}$, Eq. (27) can once more be approximated by Eq. (33), leading to Eq. (47), and Eq. (28) can again be approximated by Eq. (33), which yields

$$\tilde{\varepsilon}_d + \frac{1}{2}\tilde{U} \simeq (\varepsilon_d + \frac{1}{2}U) \exp\left[-\frac{2}{(1-r)\pi} \left(\frac{\tilde{\Gamma}}{\tilde{D}} - \frac{\Gamma}{D}\right)\right]. \quad (58)$$

Equations (47) and (58) imply that

$$\tilde{\varepsilon}_d + \frac{1}{2}\tilde{U} \simeq (\varepsilon_d + \frac{1}{2}U) \sqrt{\tilde{U}/U}. \quad (59)$$

Equations (33), (47), and (58) remain valid until either $\tilde{\Gamma}/\tilde{D}$ reaches 1 at $\tilde{D} = \tilde{D}_\Gamma$ or $(\tilde{U} + \tilde{\varepsilon}_d)/\tilde{D}$ reaches 1 at $\tilde{D} = \tilde{D}_1$. By writing $\tilde{U} + \tilde{\varepsilon}_d = \frac{1}{2}\tilde{U} + (\tilde{\varepsilon}_d + \frac{1}{2}\tilde{U})$, then employing Eqs. (47), (48), and (58), the latter condition can be recast as

$$\tilde{x}e^{-\gamma\tilde{x}/2}[\eta + e^{-\gamma\tilde{x}/2(1-r)}]^{1-r} = 1, \quad (60)$$

with \tilde{x} and γ as defined in Eqs. (49) and (50), and

$$\eta = \left(1 + \frac{2\varepsilon_d}{U}\right) \exp\left[-\frac{2\Gamma}{\pi(1-r)D}\right] \simeq 1. \quad (61)$$

Given Eq. (51), the conditions $\tilde{\Gamma}(\tilde{D}_1) < \tilde{U}(\tilde{D}_1) + \tilde{\varepsilon}_d(\tilde{D}_1) = \tilde{D}_1$ are satisfied provided that Eq. (60) has a real solution $\tilde{x} = \tilde{x}_1(\gamma) < 4/\pi\gamma$. Such solutions exist for $\gamma \lesssim \gamma_{\text{max}}(r) = (4/\pi)e^{-2/\pi}[\eta + e^{-2/\pi(1-r)}]^{1-r}$. For $\eta = 1$, there is a monotonic decrease in γ_{max} with increasing r , from $\gamma_{\text{max}}(0^+) \simeq 1.030$ to $\gamma_{\text{max}}(1^-) \simeq 0.674$, while the solution to Eq. (60) satisfies $2^{-(1-r)} \leq \tilde{x}_1 \leq 4/\pi\gamma_{\text{max}} < 1.89$.

In the regime $\tilde{D} < \tilde{D}_1$, entered with $\tilde{\varepsilon}_d = \tilde{\varepsilon}_{d,1}$, the doubly occupied impurity configuration is essentially frozen out. Now Eq. (26) can be approximated by Eq. (39), again yielding Eq. (40). This second phase of the scaling continues until one of the following conditions is met: (a) $\tilde{\varepsilon}_d = \tilde{D}$, signaling crossover into the empty-impurity region of the ASC₋ phase; (b) $\tilde{\Gamma} = \tilde{D}$, marking entry into the mixed-valence region of the ASC₋ phase; (c) $\tilde{\varepsilon}_d = -\tilde{D}$, marking entry into the local-moment regime. In case (c), the system may be mapped onto the pseudogap Kondo Hamiltonian described by Eqs. (30)–(32), which may lie in (c)(i) the ASC₋ phase, or (c)(ii) the LM phase. Integrating the poor man's scaling equations with sufficient accuracy to distinguish among all these possibilities is in general a formidable challenge.

Progress on locating the LM-ASC₋ phase boundary can be made in the limit $\gamma \ll 1$ of very weak impurity-band hybridization, where $\tilde{D}_1 \simeq U + \varepsilon_d$ and $\tilde{x}_1 = (1 + \eta)^{-(1-r)}[1 + O(\gamma)]$. Focusing for simplicity on $\eta \rightarrow 1$, one finds

$$\tilde{\varepsilon}_{d,1} \simeq \varepsilon_d + \frac{\Gamma}{(1-r)\pi} \left(\frac{U}{D}\right)^r, \quad (62)$$

and hence [via Eq. (40)]

$$\tilde{\varepsilon}_d = \varepsilon_d + \frac{\Gamma}{r\pi} \left[\frac{1}{1-r} \left(\frac{U}{D}\right)^r - \left(\frac{\tilde{D}}{D}\right)^r\right]. \quad (63)$$

In this limit of small γ , one expects only a small fractional change in the bare level energy ε_d to be required to drive the system from case (a) to case (c)(ii) of the previous paragraph. Under these circumstances, just as was done with greater rigor for $r > 1$, one can approximate the location of the phase boundary by the condition $\tilde{\varepsilon}_d(\tilde{D} = 0) = 0$, leading to

$$\varepsilon_{d,c}^+ \simeq -\frac{\Gamma}{r(1-r)\pi} \left(\frac{U}{D}\right)^r. \quad (64)$$

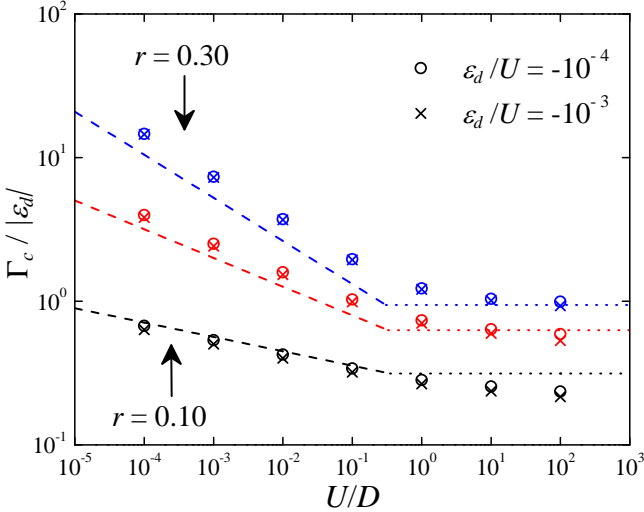


FIG. 5. Critical coupling Γ_c found using NRG (symbols) plotted as $\Gamma_c/|\varepsilon_d|$ against U/D for $\varepsilon_d/U = -10^{-4}$ and -10^{-3} and for $r = 0.1, 0.2$ and 0.3 . Also plotted are the poor man's scaling prediction of Eq. (65) for $U \ll D$ (dashed lines) and Eq. (45) for $U \gg D$ (dotted lines).

Equation (64) can be inverted such that the system is in the LM phase if $\Gamma < \Gamma_c$, where the critical coupling is given by

$$\Gamma_c = r(1-r)\pi|\varepsilon_d|\left(\frac{U}{D}\right)^{-r}. \quad (65)$$

For $U \gg D$, the evolution of $\tilde{\varepsilon}_d$ with \tilde{D} is as described by Eq. (44). For $\gamma \ll 1$, arguments similar to those given at the end of the previous section lead to the conclusion that the LM-ASC₋ boundary is given by Eq. (45).

Figure 5 shows the critical hybridization width plotted as $\Gamma_c/|\varepsilon_d|$ vs U/D for band exponents $r = 0.1, 0.2$ and 0.3 and for two values of the ratio $|\varepsilon_d|/U$ listed in legend. NRG data (symbols) are compared with the poor man's scaling predictions. For $U \ll D$, $\Gamma_c/|\varepsilon_d|$ exhibits a $(U/D)^{-r}$ dependence that is described very well by Eq. (65) (dashed lines) apart from an overall multiplicative factor that grows with increasing r . For $U \gg D$, $\Gamma_c/|\varepsilon_d|$ is almost (but not quite) a constant as predicted by Eq. (45) (dotted lines). These behaviors show that the poor man's scaling approach provides a good account of the phase boundary in the limit of strong p - h asymmetry on the impurity site.

III. ANISOTROPIC POWER-LAW KONDO MODEL

In this section, we present a poor man's scaling analysis of the phase boundary between the Kondo and local-moment (LM) phases of the Kondo model with distinct longitudinal and transverse spin-flip couplings between

the impurity and a power-law-vanishing or power-law-diverging density of states. The model is described by the Hamiltonian

$$\hat{H}_K = \hat{H}_{\text{band}} + J_z \hat{S}_z \hat{s}_z + \frac{1}{2} J_{\perp} (\hat{S}^+ \hat{s}^- + \hat{S}^- \hat{s}^+), \quad (66)$$

where \hat{H}_{band} is as given in Eq. (2) with the density of states specified in Eq. (9), and \hat{S} and $\hat{s} = N_k^{-1} \sum_{\mathbf{k}, \mathbf{k}'} \sum_{\sigma, \sigma'} c_{\mathbf{k}\sigma}^{\dagger} \frac{1}{2} \sigma_{\sigma\sigma'} c_{\mathbf{k}'\sigma'}$ (with σ being a vector of Pauli matrices) are, respectively, the spin- $\frac{1}{2}$ operators for the impurity and for conduction band electrons at the impurity site. The properties of the model are invariant under $J_{\perp} \rightarrow -J_{\perp}$, but for notational simplicity we will consider only $J_{\perp} \geq 0$.

Our focus is primarily on pseudogap cases $r > 0$, which can arise, for example, due to the low-temperature freeze-out of charge fluctuations in the Anderson-Holstein model with a power-law density of states [45]. However, in Sec. III C we briefly consider the range $-1 < r < 0$ describing bands with a generalized Van Hove singularity at the Fermi energy [22, 23].

A. Poor man's scaling equations

By generalizing Anderson's poor man's scaling treatment of the conventional ($r = 0$) Kondo problem [5], it is straightforward to extend Withoff and Fradkin's analysis of the pseudogap Kondo problem to anisotropic exchange. Under progressive reduction of the half-bandwidth from D to $\tilde{D} = D e^{-l}$, the exchange couplings (J_z, J_{\perp}) evolve to $(\tilde{J}_z, \tilde{J}_{\perp})$ according to

$$\frac{d\tilde{J}_z}{dl} = -r\tilde{J}_z + \rho_0 \tilde{J}_{\perp}^2, \quad (67a)$$

and

$$\frac{d\tilde{J}_{\perp}}{dl} = -r\tilde{J}_{\perp} + \rho_0 \tilde{J}_z \tilde{J}_{\perp}. \quad (67b)$$

On the right-hand side of each of these equations, the first term reflects the change in the density of states at the band edge (a single-particle effect), while the second term reflects the lowest-order many-body effects and is independent of r . These equations neglect all contributions beyond second-order in the exchange, and are therefore restricted in validity to situations where $|\rho_0 \tilde{J}_z| \ll 1$ and $\rho_0 \tilde{J}_{\perp} \ll 1$.

Equations (67) can be combined to obtain

$$\frac{d}{dl} (\tilde{J}_z^2 - \tilde{J}_{\perp}^2) = -2r (\tilde{J}_z^2 - \tilde{J}_{\perp}^2), \quad (68)$$

which can be integrated to yield

$$\tilde{J}_z^2 - \tilde{J}_{\perp}^2 = (J_z^2 - J_{\perp}^2) e^{-2rl}, \quad (69)$$

One sees that exchange anisotropy is irrelevant for $r > 0$ (pseudogapped systems), marginal for $r = 0$ (conventional metals), and relevant for $r < 0$ (describing a power-law divergence of the host density of states at the Fermi

energy). Equation (69) can be inserted into Eq. (67a) to obtain

$$\frac{d\tilde{J}_z}{dl} = -r\tilde{J}_z + \rho_0\tilde{J}_z^2 - \rho_0(J_z^2 - J_\perp^2)e^{-2rl}. \quad (70)$$

After the completion of the work reported in this paper, we learned of a recent poor man's scaling formulation of the power-law Kondo model with a more general anisotropic exchange coupling $J_x\hat{S}_x\hat{s}_x + J_y\hat{S}_y\hat{s}_y + J_z\hat{S}_z\hat{s}_z$ [52]. For the case $J_x = J_y = J_\perp$ considered here, the scaling equations of Ref. 52 reduce to Eqs. (67) and yield scaling trajectories fully equivalent in appearance to those plotted in Figs. 6 and 11 of this paper.

B. Pseudogapped density of states

For $r > 0$, Eqs. (67) have two stable fixed points, both isotropic as expected from Eq. (69): the weak-coupling or LM fixed point $\tilde{J}_z = \tilde{J}_\perp = 0$, and the strong-coupling or Kondo fixed point $\tilde{J}_z = \tilde{J}_\perp = \infty$ (which lies beyond the range of validity of the equations but is known to exist from nonperturbative studies). There is also a critical fixed point $\rho_0\tilde{J}_z = \rho_0\tilde{J}_\perp = r$ that lies on the boundary between the basins of attraction of the stable fixed points. The goal of this subsection is to map out the location of this boundary away from the point of SU(2) spin symmetry. In light of Eq. (69), it is clear that any starting point on the boundary flows under Eqs. (67) to the isotropic critical point first identified by Withoff and Fradkin [19], which therefore governs the low-energy physics.

For $J_z \neq 0$, one can factorize out the variation of \tilde{J}_z arising from pure density-of-states effects [i.e., the effect of the $-r\tilde{J}_z$ term on the right-hand-side of Eq. (70)] through the substitution

$$\tilde{J}_z = \tilde{j}(l) J_z e^{-rl}, \quad (71)$$

which converts Eq. (70) to

$$\frac{d\tilde{j}}{dl} = \left[\tilde{j}^2 - 1 + (J_\perp/J_z)^2 \right] \rho_0 J_z e^{-rl} \quad (72)$$

with the initial condition $\tilde{j}(0) = 1$. For any antiferromagnetic bare exchange $J_z > 0$ and any $J_\perp > 0$, Eq. (72) yields $d\tilde{j}/dl \geq 0$ so that $\tilde{j} > 1$ for all $l > 0$. If \tilde{j} remains finite as $l \rightarrow \infty$, then \tilde{J}_z vanishes as $\tilde{D} \rightarrow 0$ and the system must lie in the LM phase. On the other hand, we can associate the divergence of \tilde{j} at some value $l = l_K$ with entry into the Kondo regime around temperature $T_K = De^{-l_K}$. The boundary between the two phases is determined by the divergence of $\tilde{j}(l)$ only at $l = \infty$. For a ferromagnetic bare exchange $J_z < 0$, any $J_\perp \neq 0$ is sufficient to ensure that $\tilde{j} < 1$ for all $l > 0$. In this case, the system enters the Kondo regime if \tilde{j} changes sign and reaches $-\infty$ for some finite l_K .

For the purposes of more detailed analysis, it proves convenient to parametrize the anisotropy of the bare ex-

change couplings in terms of the variable

$$\alpha = \sqrt{|(J_\perp/J_z)^2 - 1|} \operatorname{sgn}[(J_\perp/J_z)^2 - 1], \quad (73)$$

which can range from -1 (for $J_\perp = 0$) to 0 (for $J_\perp = |J_z|$) to $+\infty$ (for $J_\perp \gg |J_z|$). Then Eq. (72) can be rewritten

$$\frac{d\tilde{j}}{dl} = (\tilde{j}^2 + \alpha|\alpha|) \rho_0 J_z e^{-rl}. \quad (74)$$

Solutions of this equation will be examined in the next two subsections.

1. Easy-plane anisotropy

In cases where $J_\perp > |J_z| > 0$, α defined in Eq. (73) is positive and Eq. (74) has the solution

$$\tilde{j}(l) = \alpha \tan \left[\operatorname{acot} \alpha + \frac{\alpha \rho_0 J_z}{r} (1 - e^{-rl}) \right]. \quad (75)$$

For antiferromagnetic bare exchange ($J_z > 0$), the Kondo phase occupies the region of parameter space in which there is a solution $0 \leq l_K < \infty$ of the equation $\tilde{j}(l_K) = \infty$, i.e.,

$$\operatorname{acot} \alpha + \frac{\alpha \rho_0 J_z}{r} > \frac{\pi}{2} \quad (76)$$

Thus, the Kondo phase extends over $J_z > J_{z,c}(\alpha)$ where

$$\rho_0 J_{z,c}(\alpha) = r \frac{\operatorname{atan} \alpha}{\alpha}. \quad (77)$$

For $\alpha \ll 1$ (weak anisotropy),

$$\rho_0 J_{z,c} \simeq r \left(1 - \frac{1}{3} \alpha^2 \right), \quad (78)$$

which reduces for $\alpha \rightarrow 0$ to the standard result [19] $\rho_0 J_{z,c} = \rho_0 J_{\perp,c} = r$. For $\alpha \gg 1$ (strong anisotropy),

$$\rho_0 J_{z,c} \simeq \frac{r\pi}{2\alpha} \left(1 - \frac{2}{\pi\alpha} \right), \quad (79)$$

which implies that the Kondo phase occupies the region $J_\perp > J_{\perp,c}$ where

$$\rho_0 J_{\perp,c} \simeq \frac{r\pi}{2} \left(1 - \frac{2}{\pi\alpha} \right). \quad (80)$$

For ferromagnetic bare exchange ($J_z < 0$), the condition for entry into the Kondo regime becomes $\tilde{j}(l_K) = -\infty$, which is met for some finite l_K provided that

$$\operatorname{acot} \alpha + \frac{\alpha \rho_0 J_z}{r} < -\frac{\pi}{2}. \quad (81)$$

Due to the dependence of α on J_z , this inequality is more likely to be satisfied for smaller values of $|J_z|$ than for

larger values. Therefore, the Kondo phase extends over the region $J_z > J_{z,c}(\alpha)$, where

$$\rho_0 J_{z,c}(\alpha) = -\frac{r}{\alpha}(\pi - \text{atan} \alpha). \quad (82)$$

For $0 < \alpha \ll 1$ (weak anisotropy),

$$\rho_0 J_{z,c} \simeq -\frac{r\pi}{\alpha} \left(1 - \frac{\alpha}{\pi}\right), \quad (83)$$

while for $\alpha \gg 1$ (strong anisotropy),

$$\rho_0 J_{z,c} \simeq -\frac{r\pi}{2\alpha} \left(1 + \frac{2}{\pi\alpha}\right), \quad (84)$$

so the Kondo phase spans $J_\perp > J_{\perp,c}(\alpha)$ where

$$\rho_0 J_{\perp,c}(\alpha) \simeq \frac{r\pi}{2} \left(1 + \frac{2}{\pi\alpha}\right). \quad (85)$$

2. Easy-axis anisotropy

For $|J_z| > J_\perp > 0$, α defined in Eq. (73) satisfies $-1 < \alpha < 0$ and the solution of Eq. (74) is

$$\tilde{j}(l) = \alpha \coth \left[\text{atanh} \alpha - \frac{\alpha \rho_0 J_z}{r} (1 - e^{-rl}) \right]. \quad (86)$$

For antiferromagnetic bare exchange ($J_z > 0$), the Kondo phase spans the region in which

$$\text{atanh} \alpha - \frac{\alpha \rho_0 J_z}{r} > 0, \quad (87)$$

i.e., the region $J_z > J_{z,c}$ where

$$\rho_0 J_{z,c} = r \frac{\text{atanh} \alpha}{\alpha}. \quad (88)$$

For $|\alpha| \ll 1$ (weak anisotropy),

$$\rho_0 J_{z,c} \simeq r \left(1 + \frac{1}{3}\alpha^2\right) \quad (89)$$

while for $\alpha \rightarrow -1^+$ (strong anisotropy),

$$\rho_0 J_{z,c} \simeq \frac{r}{2} \ln \frac{2}{1 + \alpha}. \quad (90)$$

For $J_z < -J_\perp < 0$, it is straightforward to see that $|\alpha| \leq \tilde{j}(l) < 1$ for all $l > 0$ and the system always lies in the LM phase.

3. XY exchange anisotropy

In the special case $J_z = 0$ of pure-XY bare exchange coupling, the scaling in Eq. (71) can be replaced by

$$\tilde{J}_z = \tilde{j}_\perp(l) J_\perp e^{-rl}, \quad (91)$$

which converts Eq. (70) to

$$\frac{d\tilde{j}_\perp}{dl} = (\tilde{j}_\perp^2 + 1) \rho_0 J_\perp e^{-rl} \quad (92)$$

with initial condition $\tilde{j}_\perp(0) = 0$. The equation has solution

$$\tilde{j}_\perp(l) = \tan \left[\frac{\rho_0 J_\perp}{r} (1 - e^{-rl}) \right]. \quad (93)$$

In the Kondo phase, there must be an l_K ($0 < l_K < \infty$) such that $\tilde{j}_\perp(l_K) = \infty$, a condition that is satisfied for $J_\perp > J_{\perp,c}$ where

$$\rho_0 J_{\perp,c} = \frac{r\pi}{2}. \quad (94)$$

As one would expect, this result coincides with the limits $\alpha \rightarrow \infty$ of Eqs. (80) and (85).

4. Comparison with NRG

The preceding results for the location of the phase boundary as a function of α and the sign of J_z can be re-expressed as the statement that for any value of J_z , the Kondo phase occupies the region $J_\perp > J_{\perp,c}(J_z)$, where $J_{\perp,c}$ is a monotonically decreasing function of J_z that has the following limiting forms:

$$\rho_0 J_{\perp,c} \simeq \rho_0 |J_z| \left[1 + \frac{1}{2} \left(\frac{r\pi}{\rho_0 J_z} \right)^2 \right] \quad \text{for } 1 \gg -\rho_0 J_z \gg r\pi, \quad (95a)$$

$$\rho_0 J_{\perp,c} \simeq r\pi/2 - 2\rho_0 J_z/\pi \quad \text{for } \rho_0 |J_z| \ll r, \quad (95b)$$

$$\rho_0 J_{\perp,c} \simeq r - \frac{1}{2}(\rho_0 J_z - r) \quad \text{for } |\rho_0 J_z - r| \ll r/3, \quad (95c)$$

$$\rho_0 J_{\perp,c} \simeq 2\rho_0 J_z \exp(-\rho_0 J_z/r) \quad \text{for } r \ll \rho_0 J_z \ll 1. \quad (95d)$$

In the limit $r \rightarrow 0$, these expressions reproduce the standard result [5] $J_{\perp,c} = |J_z| \theta(-J_z)$. The purpose of this section is to test these statements based on poor man's scaling against nonperturbative NRG calculations.

Scaling trajectories for the pseudogap Kondo model, calculated via numerical iteration of Eqs. (67) with different starting parameters, are plotted in Figs. 6(a) and 6(b) for $r = 0.1$ and $r = 0.3$, respectively. Solid lines show trajectories that flow to the fixed points of the model. Arrows on some of the trajectories show the direction of flow of the couplings under reduction of the half-bandwidth D . The phase boundary (thick line) separating the basins of attraction of the LM fixed point ($\rho_0 J_z = \rho_0 J_\perp = 0$) and the Kondo fixed point ($\rho_0 J_z = \rho_0 J_\perp = \infty$) was found by (a) reversing the flow of Eqs. (67) and (b) choosing starting parameters very close to the critical coupling $\rho_0 J_{z,c} = \rho_0 J_{\perp,c} = r$ and lying on either side of the the

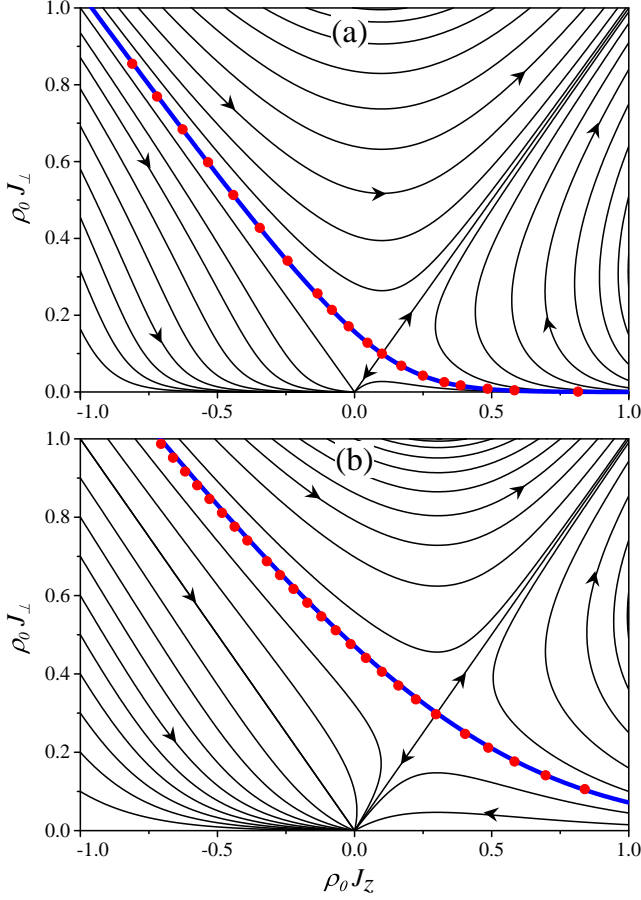


FIG. 6. Scaling trajectories for the pseudogap Kondo model with (a) $r = 0.1$, (b) $r = 0.3$, calculated via numerical iteration of Eqs. (67). Arrows indicate the direction of flow under reduction of the half-bandwidth D . Thick lines show trajectories that flow to the critical fixed point, thereby defining the boundary between the LM and Kondo phases. Circles represent points on the phase boundary as determined using the NRG, with all J_z and J_\perp values for given r rescaled by the same multiplicative factor, chosen so that the isotropic boundary point is located at $\rho_0 J_z = \rho_0 J_\perp = r$.

trajectory $J_z = J_\perp$. For comparison, NRG data for the phase boundary (circles) are shown, with all values of J_z and $J_{\perp,c}$ rescaled by the multiplicative factor that places the isotropic critical point at $\rho_0 J_z = \rho_0 J_{\perp,c} = r$. This r -dependent multiplicative factor is introduced to account both for a known reduction in hybridization arising from the NRG discretization [31, 48] and for the effect of higher-order terms omitted from the poor man's scaling equations (67), which shift the isotropic critical point from $\rho_0 J_c = r$ to $\rho_0 J_c = f(r) \simeq r(1 + r/2)$ [20]. Figure 6 shows that poor man's scaling does an excellent job of reproducing the shape of the phase boundary over the entire region of couplings $\rho_0 |J_z| < 1$, $\rho_0 J_\perp < 1$.

A more rigorous test of the poor man's scaling is provided by Figs. 7–10, which compare $\rho_0 J_{\perp,c}$ vs $\rho_0 J_z$ calculated for one of the limiting cases in Eqs. (95) (solid

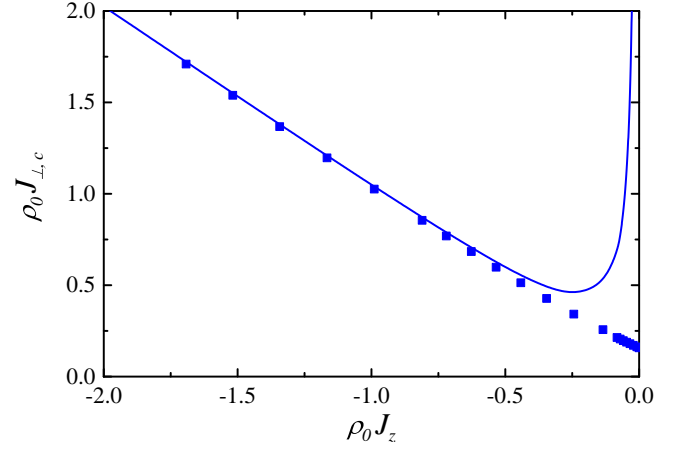


FIG. 7. Pseudogap Kondo model phase boundary $\rho_0 J_{\perp,c}$ vs $\rho_0 J_z$ for $r = 0.1$, comparing NRG results (symbols) with the poor man's scaling prediction for $\rho_0 J_z \ll -r\pi$ as given in Eq. (95) (line).

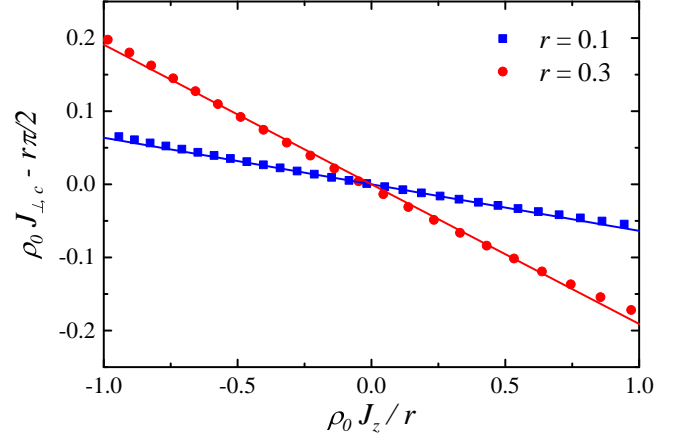


FIG. 8. Pseudogap Kondo model phase boundary plotted as $\rho_0 J_{\perp,c} - r\pi/2$ vs $\rho_0 J_z/r$ for $r = 0.1$ and $r = 0.3$, comparing NRG results (symbols) with the poor man's scaling prediction for $\rho_0 |J_z| \ll r$ as given in Eq. (95b) (lines).

lines) with their NRG counterparts (symbols). The NRG results are again scaled so that the isotropic critical point is at $\rho_0 J_z = \rho_0 J_{\perp,c} = r$.

Figure 7 plots the critical coupling $\rho_0 J_{\perp,c}$ for $r = 0.1$ over a range of ferromagnetic exchange couplings $\rho_0 J_z < 0$. Although the perturbative scaling analysis is not strictly valid for $\rho_0 J_z \lesssim -1$, Eq. (95a) captures surprisingly well the variation of $\rho_0 J_{\perp,c,\text{NRG}}$ at least as far as $\rho_0 J_z = -1.7$. For $r = 0.3$, the restriction $\rho_0 J_z \ll -r\pi$ rules out the applicability of Eq. (95a) anywhere within the range of validity of the scaling equations, so no results are shown for this case.

In Fig. 8, the critical coupling is plotted as $\rho_0 J_{\perp,c} - r\pi/2$ versus $\rho_0 J_z/r$ near $\rho_0 J_z = 0$. The NRG results are well reproduced by the poor man's scaling prediction Eq. (95b) over its entire range of validity $\rho_0 |J_z| \lesssim r$. Figure

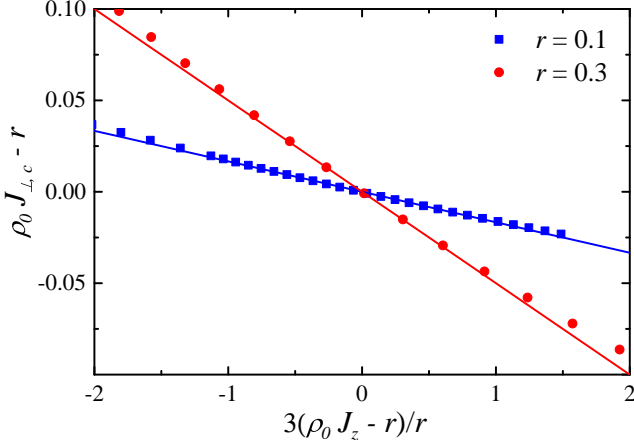


FIG. 9. Pseudogap Kondo model phase boundary plotted as $\rho_0 J_{\perp,c} - r$ vs $3(\rho_0 J_z - r)/r$ for $r = 0.1$ and $r = 0.3$, comparing NRG results (symbols) with the poor man's scaling prediction for $\rho_0 |J_z - r| \ll r/3$ as given in Eq. (95c) (lines).

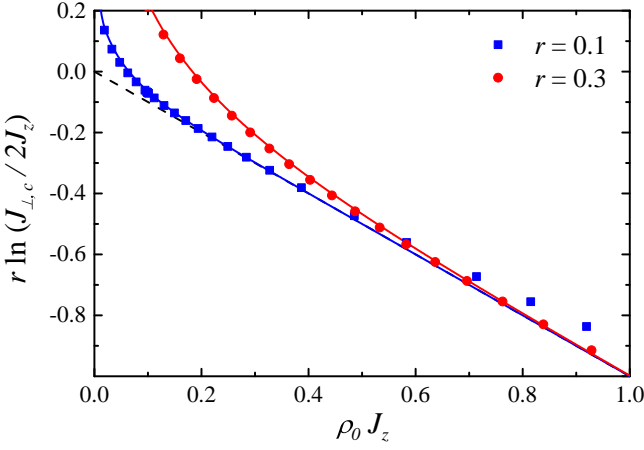


FIG. 10. Pseudogap Kondo model phase boundary plotted as $r \ln(J_{\perp,c}/2J_z)$ vs $\rho_0 J_z$ for $r = 0.1$ and $r = 0.3$, comparing NRG results (symbols) with the poor man's scaling prediction obtained via numerical solution of Eq. (88) (solid lines) and the asymptotic form for $\rho_0 J_z \gg r$ from Eq. (95d) (dashed line).

9 focuses on the vicinity of the isotropic critical point at $\rho_0 J_z = \rho_0 J_{\perp,c} = r$, plotting the critical coupling as $\rho_0 J_{\perp,c} - r$ vs $3(\rho_0 J_z - r)/r$. The scaling prediction in Eq. (95c) closely reproduces the NRG results over the range $\rho_0 |J_z - r| \ll r/3$.

Lastly, Fig. 10 plots the critical coupling as $r \ln(J_{\perp,c}/2J_z)$ versus $\rho_0 J_z$ for $0 \leq \rho_0 J_z \leq 1$. We find that the NRG results closely follow the asymptotic form for $r \ll \rho_0 J_z \ll 1$ [Eq. (95d), dashed line] over the range $0.2 \lesssim \rho_0 J_z \lesssim 0.7$ for $r = 0.1$ and over $0.6 \lesssim \rho_0 J_z \lesssim 1$ for $r = 0.3$. There are minor deviations from the asymptotic form as $\rho_0 J_z$ nears 1 due to perturbative effects beyond second order. We have also plotted the poor man's scaling prediction obtained via numerical solution of Eq. (88)

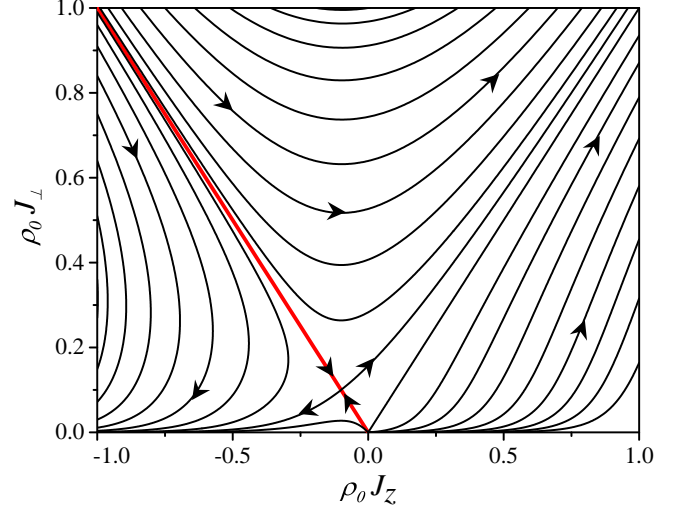


FIG. 11. Scaling trajectories for the pseudogap Kondo model with $r = -0.1$, representing a divergence of the density of states at the Fermi energy. Arrows indicate the direction of flow under reduction of the half-bandwidth D . Thick lines show trajectories that flow to the critical point, defining the phase boundary between the ferromagnetic and Kondo phases.

(solid lines), which can be seen to describe correctly the deviation of $J_{\perp,c,\text{NRG}}$ near $J_z = 0$ from its $\rho_0 J_z \gg r$ asymptote.

The overall conclusion from Figs. 6–10 is that the poor man's scaling approach provides an excellent account of the location of the boundary between the Kondo and local-moment phases of the spin-anisotropic pseudogap Kondo model under conditions of strict p - h symmetry.

C. Divergent density of states

Coupling a Kondo impurity to a fermionic density of states that diverges at the Fermi level in a manner described by Eq. (9) with $r < 0$ has been shown to yield rich physics including nontrivial quantum phase transitions occurring for ferromagnetic exchange couplings $J < 0$ [22, 23]. The poor man's scaling analysis of the spin-anisotropic Kondo model applies also to cases $r < 0$. Examination of Eqs. (67) show that the poor man's scaling trajectories for $r < 0$ can be obtained from those for band exponent $|r| > 0$ through the simple replacements $r \rightarrow -r$, $\tilde{J}_z \rightarrow -\tilde{J}_z$. This mapping implies that the scaling trajectories for $r < 0$ should be reflections of those for $r > 0$ about the axis $J_z = 0$ with reversal of the direction of flow arrows. This is illustrated in Fig. 11, which plots the scaling trajectories for a representative case $r = -0.1$ over the range of exchange couplings $-1 < \rho_0 J_z < 1$ and $0 < \rho_0 J_{\perp} < 1$. Arrows indicate the direction of flow of couplings with decreasing effective half-bandwidth. The model has three stable fixed points: a ferromagnetic

fixed point at $(\rho_0 J_z, \rho_0 J_\perp) = (-\infty, 0)$ where the impurity is locked into a many-body spin triplet with the conduction band, the symmetric strong-coupling fixed point at $(\rho_0 J_z, \rho_0 J_\perp) = (\infty, \infty)$, and an intermediate coupling fixed point at $(\rho_0 J_z, \rho_0 J_\perp) = (-|r|, |r|)$. The phase boundary (thick lines) separating the ferromagnetic and strong-coupling phase is given by the condition $J_z = -|J_\perp|$, which is entirely consistent with NRG results for the model (data not shown in Fig. 11).

IV. DISCUSSION

In this work, we have extended the poor man's scaling approach to analyze phase boundaries in variants of the Anderson and Kondo impurity models in which a power-law vanishing or divergence of the host density of states at the Fermi energy gives rise to a nontrivial phase diagram featuring local-moment and Kondo-screened ground states. In the regime of weak-to-moderate impurity-band couplings where poor man's scaling is expected to be valid, the predicted locations of the phase boundaries are generally in excellent qualitative and good quantitative agreement with those obtained using the numerical renormalization group (NRG). Although the NRG remains the most reliable technique for treating power-law quantum impurity problems, the scaling approach has the advantages that it is much more intuitive and it can clarify algebraically the functional dependence of the critical impurity-host coupling on other model parameters. Thus, poor man's scaling retains considerable value even for quantum impurity problems where two or more competing RG flows give rise to different possible infrared-stable fixed points separated by quantum phase transitions.

Despite its successes demonstrated in Secs. II and III, poor man's scaling has two significant limitations. First, and more obviously, the approach is perturbative in the impurity-band coupling and is unable to describe physics at strong coupling. In the pseudogap Anderson model, a reliable calculation of the critical hybridization based on poor man's scaling alone is possible for all $r > 0$ only for $0 < -\varepsilon_d \ll U/2$ (on the ASC_- side) or $0 < U + \varepsilon_d \ll U/2$ (on the ASC_+ side). Near the p - h -symmetric point $\varepsilon_d = -\frac{1}{2}U$, the method breaks down for $r \gtrsim \frac{1}{3}$. This is

clear to see for $r > \frac{1}{2}$ because $\Gamma_c(U, \varepsilon_d)$ diverges as $\varepsilon_d \rightarrow -\frac{1}{2}U$ [see Fig. 1(b)] and therefore any phase boundary lies outside the perturbative regime (as is also the case for the corresponding Kondo model). For $\frac{1}{3} \lesssim r < \frac{1}{2}$, $\Gamma_c(U, \varepsilon_d)$ remains finite for all $-U < \varepsilon_d < 0$ [see Fig. 1(b)] but, as discussed in Ref. 31 and in Sec. IID above, the strong-coupling phases are accessed directly from mixed valence, and in such cases we have been unable to find a scaling criterion for locating the phase boundaries.

A second deficiency of poor man's scaling is that it does not seem to be capable of reproducing the full RG fixed-point structure identified using the NRG [31]. Scaling Eq. (28) and its counterpart $d\tilde{K}/d\tilde{D} = r\tilde{K}/\tilde{D}$ for the potential scattering in the pseudogap Kondo model both indicate that p - h asymmetry is an irrelevant perturbation about the symmetric plane $\tilde{\varepsilon}_d = -\frac{1}{2}\tilde{U}$. This is consistent with NRG results for band exponents on the range $0 < r \leq r^* \simeq 3/8$, where a single p - h -symmetric quantum critical point (QCP) governs the physics all over the phase boundary between the LM and strong-coupling phases shown in Fig. 1(a). However, there also exists a range $r^* < r < \frac{1}{2}$ in which the boundary between the LM phase and each strong-coupling phase (SSC , ASC_- , and ASC_+) is governed by a different QCP. Within this second range of band exponents, poor man's scaling cannot detect that p - h asymmetry is a relevant perturbation that causes flow from the symmetric QCP to one or the other of the two asymmetric QCPs [as illustrated schematically for the pseudogap Kondo model in Fig. 16(b) of Ref. 31]. This is a quite subtle aspect of the pseudogap Kondo and Anderson models that even much more sophisticated RG treatments are unable to fully capture [38].

ACKNOWLEDGMENTS

This work has been supported in part by NSF MWN Grants No. 0710540 (M.C., K.I.) and No. DMR-1107814 and No. DMR-1508122 (T.C., K.I.). A.M. was supported by the University of Florida REU Site in Materials Physics under NSF Grant No. DMR-1156737 with additional support from the US Department of Defense. We thank E. Kogan for bringing Ref. 52 to our attention and for useful discussions.

-
- [1] A. C. Hewson, *The Kondo Problem to Heavy Fermions* (Cambridge University Press, Cambridge, UK, 1993).
 - [2] A. A. Abrikosov and A. A. Migdal, *J. Low Temp. Phys.* **3**, 519 (1970).
 - [3] M. Fowler and A. Zawadowski, *Sol. St. Commun.* **9**, 471 (1971).
 - [4] P. W. Anderson, G. Yuval, and D. R. Hamann, *Phys. Rev. B* **1**, 4464 (1970).
 - [5] P. W. Anderson, *J. Phys. C* **3**, 2436 (1970).
 - [6] K. G. Wilson, *Rev. Mod. Phys.* **47**, 773 (1975).
 - [7] J. H. Jefferson, *J. Phys. C* **10**, 3589 (1977).
 - [8] F. D. M. Haldane, *Phys. Rev. Lett.* **40**, 416 (1978).
 - [9] Ph. Nozières and A. Blandin, *J. Phys. (Paris)* **41**, 193 (1980).
 - [10] M. Sigrist and K. Ueda, *Rev. Mod. Phys.* **63**, 239 (1991).
 - [11] T. Timusk and B. Statt, *Rep. Prog. Phys.* **62** 61 (1999).
 - [12] For reviews, see G. Nimtz, B. Schlichter, "Narrow-Gap Lead Salts," in *Narrow-Gap Semiconductors*, Springer Tracts in Modern Physics, Vol. 98, ed. G. Höhler (Springer-Verlag, Berlin, 1983), p. 1; R. Dornhaus and G. Nimtz,

- “The Properties and Applications of the $\text{Hg}_{1-x}\text{Cd}_x\text{Te}$ Alloy System,” *ibid.*, p. 119.
- [13] B. A. Volkov and O. A. Pankratov, *Pis'ma Zh. Eksp. Teor. Fiz.* **42**, 145 (1985) [*JETP Lett.* **42**, 178 (1985)].
- [14] D. P. DiVincenzo and E. J. Mele, *Phys. Rev. B* **29**, 1685 (1984).
- [15] G. W. Semenoff, *Phys. Rev. Lett.* **53**, 2449 (1984).
- [16] A. H. Castro Neto, F. Guinea, N. M. R. Peres, K. S. Novoselov, and A. K. Geim, *Rev. Mod. Phys.* **81**, 109 (2009).
- [17] A. W. W. Ludwig, M. P. A. Fisher, R. Shankar, and G. Grinstein, *Phys. Rev. B* **50**, 7526 (1994).
- [18] O. Motrunich, K. Damle, and D. A. Huse, *Phys. Rev. B* **65**, 064206 (2002).
- [19] D. Withoff and E. Fradkin, *Phys. Rev. Lett.* **64**, 1835 (1990).
- [20] K. Ingersent, in “Proceedings of Physical Phenomena at High Magnetic Fields-II”, edited by Z. Fisk et al. (World Scientific Publishing Company, Singapore, 1996), pp. 179–184.
- [21] C. Gonzalez-Buxton and K. Ingersent *Phys. Rev. B* **54**, R15614 (1996).
- [22] M. Vojta and R. Bulla, *Eur. Phys. J. B* **28**, 283 (2002).
- [23] A. K. Mitchell and L. Fritz, *Phys. Rev. B* **88**, 075104 (2013).
- [24] L. S. Borkowski and P. J. Hirschfeld, *Phys. Rev. B* **46**, 9274 (1992); *J. Low. Temp. Phys.* **96**, 185 (1994).
- [25] C. R. Cassanello and E. Fradkin, *Phys. Rev. B* **53**, 15079 (1996).
- [26] M. Vojta, *Phys. Rev. Lett.* **87**, 097202 (2001).
- [27] A. Polkovnikov, *Phys. Rev. B* **65**, 064503 (2002).
- [28] K. Chen and C. Jayaprakash, *J. Phys.: Condens. Matter* **7**, L491 (1995).
- [29] K. Ingersent, *Phys. Rev. B* **54**, 11936 (1996).
- [30] R. Bulla, Th. Pruschke, and A. C. Hewson, *J. Phys.: Condens. Matter* **9**, 10463 (1997).
- [31] C. Gonzalez-Buxton and K. Ingersent, *Phys. Rev. B* **57**, 14254 (1998).
- [32] M. Vojta and R. Bulla, *Phys. Rev. B* **65**, 014511 (2001).
- [33] K. Ingersent and Q. Si, *Phys. Rev. Lett.* **89**, 076403 (2002).
- [34] J. H. Pixley, S. Kirchner, K. Ingersent, and Q. Si, *Phys. Rev. Lett.* **109**, 086403 (2012).
- [35] T. Chowdhury and K. Ingersent *Phys. Rev. B* **91**, 035118 (2015).
- [36] M. Kirčan and M. Vojta, *Phys. Rev. B* **69**, 174421 (2004).
- [37] M. Vojta and L. Fritz, *Phys. Rev. B* **70**, 094502 (2004).
- [38] L. Fritz and M. Vojta, *Phys. Rev. B* **70**, 214427 (2004).
- [39] D. E. Logan and M. T. Glossop, *J. Phys.: Condens. Matter* **12**, 985 (2000).
- [40] R. Bulla, M. T. Glossop, D. E. Logan and T. Pruschke, *J. Phys.: Condens. Matter* **12**, 4899 (2000).
- [41] M. T. Glossop and D. E. Logan, *J. Phys.: Condens. Matter* **15**, 7519 (2003).
- [42] D. E. Logan, M. P. Eastwood, and M. A. Tusch, *J. Phys.: Condens. Matter* **10**, 2673 (1998).
- [43] P. W. Anderson, *Phys. Rev.* **124**, 41 (1961).
- [44] The hybridization *function* is denoted by the symbol $\bar{\Gamma}$ to distinguish it from the hybridization *width* Γ appearing on the right-hand side of Eq. (8).
- [45] M. Cheng and K. Ingersent, *Phys. Rev. B* **87**, 075145 (2013).
- [46] J. R. Schrieffer and P. A. Wolff, *Phys. Rev.* **149**, 491 (1966).
- [47] Reference 45 states incorrectly that meeting the conditions for case (5) necessarily results in entry into a strong-coupling phase.
- [48] H. R. Krishna-murthy, J. W. Wilkins, and K. G. Wilson, *Phys. Rev. B* **21**, 1003 (1980); **21**, 1044 (1980).
- [49] R. Bulla, T. A. Costi, and Th. Pruschke, *Rev. Mod. Phys.* **80**, 395 (2008).
- [50] The impurity contribution to a physical property is defined in the standard manner (see, e.g., Ref. 48) as the difference between the total value of the property for the system including the impurity and the total value of the same property for the host alone.
- [51] We work in units where $k_B = g\mu_B = \hbar = 1$.
- [52] E. Kogan, K. Noda, and S. Yunoki, *Phys. Rev. B* **95**, 165412 (2017).